Materials Advances

ROYAL SOCIETY OF CHEMISTRY

REVIEW

View Article Online
View Journal | View Issue

Check for updates

Cite this: *Mater. Adv.*, 2023, 4, 5094

Response surface methodology: a powerful tool for optimizing the synthesis of metal sulfide nanoparticles for dye degradation

Zeshan Ali Sandhu,*[a] Muhammad Asam Raza,[a] Umme Farwa,[a] Samia Nasr,[b] Ibrahim Sayed Yahia,[bcde] Seerat Fatima,[a] Mehmuna Munawar,[a] Yousra Hadayet,[a] Sufyan Ashraf[a] and Haseeb Ashraf[a]

Received 10th July 2023,
Accepted 2nd September 2023

DOI: 10.1039/d3ma00390f

rsc.li/materials-advances

Metal sulfide nanoparticles (MSNs) have attracted significant attention due to their unique optical, electronic, and catalytic properties. These nanomaterials have great potential for many applications, such as solar cells, sensors, and environmental remediation. In particular, MSNs have demonstrated promising results in the degradation of dyes, which are hazardous pollutants commonly released by industries (textiles, leather, paper, and plastics). This review article provides a comprehensive overview of recent advancements in the synthesis of MSNs and their application in dye degradation. Two optimization approaches, namely, conventional and response surface methodology (RSM), are discussed in detail, highlighting their advantages and limitations. The conventional approach involves varying one parameter at a time, while the RSM approach uses statistical and mathematical tools to model and analyze the relationship between multiple variables and their effects on the desired response. This article also highlights recent research on optimizing the synthesis conditions for various MSNs, such as zinc sulfide (ZnS), copper sulfide, and cadmium sulfide (CdS) using both conventional and RSM approaches. Additionally, this article presents a discussion on the photocatalytic performance of MSNs in the degradation of various organic dyes, including azo, triphenylmethane, and anthraquinone dyes. Overall, this review serves as a valuable resource for researchers working in the field of nanotechnology and environmental remediation.

1. Introduction

In recent years, the ever-increasing demand for advanced materials has led to the development of metal sulfide nanoparticles (MSNs) due to their unique optical, electronic, and catalytic properties.[1,2] These materials are being used in solar cells, sensors, and environmental remediation.[3] There are many ways to synthesize MSNs, such as chemical precipitation, hydrothermal, sol–gel, and solvothermal[4–9] methods. Each method has its advantages and limitations which affect the morphology, particle size, and overall performance of the synthesized nanoparticles.[10] Among the numerous categories of sulfide photocatalysts,[11] NiS_2, a semiconductor, has unique electrical, optical, and magnetic characteristics that make it useful in a variety of fields.[12] NiS_2 has a small band gap of approximately 0.3 eV, which allows it to capture light in the visual range and be used in photocatalytic processes.[13,14] Chen *et al.* (2020) synthesized facile NiS_2, which serves as an effective catalyst, enhancing the photocatalytic efficiency of g-C_3N_4 in H_2 production. A simple, low-temperature (80 °C) impregnation technique was devised for NiS_2/g-C_3N_4 photocatalyst creation. In recycling tests, NiS_2/g-C_3N_4(3 wt%) demonstrated consistent, high-performance photocatalytic H_2 generation under visible light.[15] The activity of metal sulfides can sometimes be limited due to factors such as poor conductivity, insufficient surface area, and inadequate stability. Various approaches have been developed to enhance the activity of metal sulfides.[16] Fig. 1 illustrates the optimization strategies for enhancing metal sulfide system activity.

Similarly, the preferred substance for photocatalytic and hydrogen evolution has been cobalt sulfide. This material can

---

[a] Department of Chemistry, Hafiz Hayat Campus, University of Gujrat, Gujrat, Pakistan. E-mail: asamgcu@yahoo.com
[b] Research Center for Advanced Materials Science (RCAMS), King Khalid University, Abha 61413, P.O. Box 9004, Saudi Arabia
[c] Laboratory of Nano-Smart Materials for Science and Technology (LNSMST), Department of Physics, Faculty of Science, King Khalid University, P.O. Box 9004, Abha, Saudi Arabia
[d] Nanoscience Laboratory for Environmental and Biomedical Applications (NLEBA), Semiconductor Lab., Metallurgical Lab.1., Department of Physics, Faculty of Education, Ain Shams University, Roxy, Cairo 11757, Egypt
[e] Center of Medical and Bio-Allied Health Sciences Research (CMBHSR), Ajman University, Ajman, United Arab Emirates

be artificially tailored for the elimination of organic pigments *via* visible light photocatalysis and adsorption by shrinking its size to the nanodomain. This material's band gap, phase, and shape can all be adjusted in this way.[17] Efficient CoS_2, Co_3S_4, and Co_9S_8 hollow nanospheres (HNSs) were synthesized by Li *et al*. (2020) for use as peroxymonosulfate (PMS) activators in ciprofloxacin[18] degradation. The CoS_2 HNS/PMS system's performance was investigated by varying operating parameters. CoS_2 HNSs demonstrated strong catalytic activity across a pH range of 3–10. At an initial pH of 8.0, 10 mg L^{-1} CIP was entirely removed by CoS_2 HNSs within 3 minutes, achieving 62.6% CIP mineralization.[19] Comparably, as a member of the family of metal sulfides, cadmium sulfide (CdS) is an intrinsic n-type semiconductor substance. With its narrow band gap energy (2.42 eV), CdS is a perfect visible photocatalyst in the visible region.[20,21] Fig. 2 presents the hydrothermal treatment for the synthesis of CdS nanoflowers. The energy bands of some of the most extensively researched metal sulfides are presented in Fig. 3.

The introduction of large amounts of dyes into both natural water and waste water treatment systems results from the discharge of various dyes from various sources, such as the paper and pulp, textile and intermediate industries.[22,23] One of the critical applications of MSNs is in the degradation of dyes, which are hazardous pollutants. The presence of dyes in aquatic ecosystems can cause severe damage to the environment and aquatic life, making it crucial to explore effective techniques for dye removal.[24] Physical, chemical, and biological

Zeshan Ali Sandhu

Zeshan Ali Sandhu is a distinguished scientific researcher and scholar in the field of chemistry holding an MPhil degree in chemistry from the University of Gujrat. His academic journey has been marked by exceptional dedication and a passion for advancing the frontiers of scientific knowledge. Zeshan exhibited a keen aptitude for practical application of the theoretical concepts. He has expertise spanning a variety of domains, including photocatalysis, electrocatalysis, energy storage devices, and environment remediation. His interdisciplinary approach and holistic understanding of these areas showcase a unique ability to connect diverse scientific principles.

Muhammad Asam Raza

Dr Muhammad Asam Raza is a distinguished researcher and academician with a strong background in the field of chemistry. He earned his PhD in chemistry from GC University Lahore, Currently, Dr Raza holds the esteemed position of Associate Professor at the University of Gujrat in Pakistan. His research journey has been marked by a profound focus on synthesis of new molecules and their application related to medicinal chemistry. Driven by a commitment to advancing scientific knowledge, he is working on the synthesis of nanomaterials for industrial and environmental applications. Dr Raza's contributions to the academic community are exemplified by his impressive publication record, which boasts more than 100 articles in reputed journals. Beyond his research endeavor, Dr Raza has generously shared his expertise by serving as reviewers for numerous esteemed scientific journals.

Umme Farwa

Umme Farwa received her Master's of Philosophy degree from the Department of Chemistry, University of Gujrat, Pakistan in 2021. She is currently doing her PhD in chemistry. Her present research interests are synthesis of heterocyclic organic compounds, nanomaterials, treatment of wastewater, bioenergy production, microbial community analysis, phytotoxity studies, computational studies, and pharmaceutical applications.

Sufyan Ashraf

Sufyan Ashraf is a dedicated young researcher pursuing an MPhil in chemistry at the University of Gujrat, Pakistan. His research focuses on the fascinating realm of nanomaterials and their versatile applications in energy storage, biological systems, and photocatalysis. Sufyan's passion for pushing the boundaries of knowledge in these domains drives his commitment to scientific exploration and innovation. Sufyan Ashraf's dedication to research and his promising contributions make him a rising star in the world of chemistry and nanotechnology

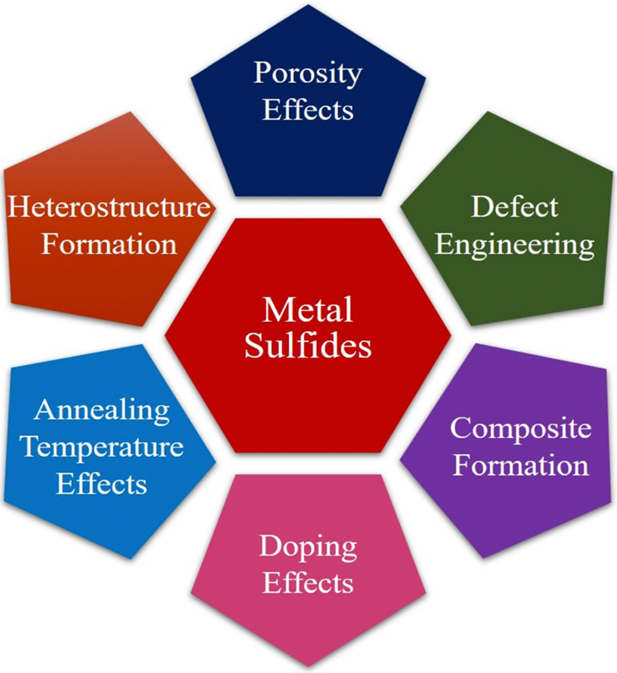

Fig. 1 Systematic methods for boosting performance in metal sulfide systems.

approaches have been developed to minimize the amount of toxins in the environment.[25] However, these methods were ineffective because the toxins had not been broken down. Instead, they were just turned into other species, which led to more pollution. In recent years, MSNs have gained interest as photocatalysts for the removal of different organic dyes.[26] The use of nanoscale catalysis and photocatalysis with nanoparticles (NPs), nanowires (NWs), or nanotubes (NTs) in wastewater treatment processes has recently shown promise in addressing some of the key issues related to heavy metals, pigments, and contaminants. The size and shape of nanoparticles play an important role in photocatalytic applications.[27,28]

Due to heavy water contamination from different industries, scholars and scientists have redirected their attention towards the exploration and advancement of effective and environmentally friendly approaches to eliminate pollutants.[29] Mostly, the photocatalytic reaction is optimized using the conventional kinetic approach, which investigates the effect of reaction parameters (including photocatalyst concentration, dye molecule concentration, irradiation time, and pH) on the response by varying one reaction parameter and measuring its effect on degradation while keeping all other reaction parameters constant.[30] Using traditional trial-and-error methods is often a long process that uses a lot of resources and may not lead to the desired results. Recently, an innovative technique for the optimization of these photocatalytic processes called response surface methodology (RSM) has evolved. This method makes use of quantitative and statistical models. This optimization method assumes that all response factors are independent of each other and have no connection.[31] As it includes interaction factors that take the connection between response parameters into consideration, this method is better than the traditional optimization method. Because of this sophisticated method, the reaction is further optimized.[32] The present discourse aims to elucidate the profound importance of response surface methodology (RSM), a statistical and mathematical approach that facilitates the methodical enhancement of intricate processes.[33] The utilization of RSM facilitates the systematic manipulation of various factors that impact the synthesis process, thereby enabling a comprehensive examination of their interrelationships. This approach proves invaluable in the identification of optimal conditions that yield improved properties of nanoparticles for the purpose of dye degradation.[34]

Haseeb Ashraf

Haseeb Ashraf is an MPhil chemistry scholar at the University of Gujrat, Pakistan. Haseeb's expertise encompasses nanoparticle synthesis, cyclic voltammetry, microbial community analysis, microbial fuel cells and phytotoxicity studies. With a commitment to bridging theory and application, he is poised to make meaningful contributions to the fields of electrochemistry and interdisciplinary research.

Recent research has focused on adjusting the nanostructure of metal sulfide nanoparticles to improve their photocatalytic activity. The surface area and light absorption characteristics are influenced by size, shape, and morphology. One option is to create hierarchical structures, such as core–shell or heterostructure topologies, which encourage charge separation and the use of a wider spectrum of light.[35,36] Doping metal sulfide nanoparticles with different elements may improve their catalytic capabilities significantly. Incorporating transition metals or nonmetals, for example, may enhance charge carrier mobility and increase light absorption. Metal sulfides with varied compositions may also be allowed to control their bandgap, resulting in increased visible light utilization and photocatalytic activity.[37] Surface engineering holds significance in enhancing catalytic activity. Surface modifications such as co-catalysts, organic ligands, or plasmonic nanoparticles may improve charge transfer kinetics while decreasing recombination rates. These changes also improve the nanoparticles' durability under strong reaction conditions.[38] The creation of heterojunctions between metal sulfide nanoparticles and other semiconductors or materials, such as graphene, improves charge carrier separation and migration. This material synergy results in excellent electron–hole separation and enhanced photocatalytic activity.[39]

The review offers a thorough understanding of metal sulfide nanoparticles, their synthesis methods, the mechanisms involved in dye degradation, and the effectiveness of RSM as a powerful statistical tool for optimizing the parameters

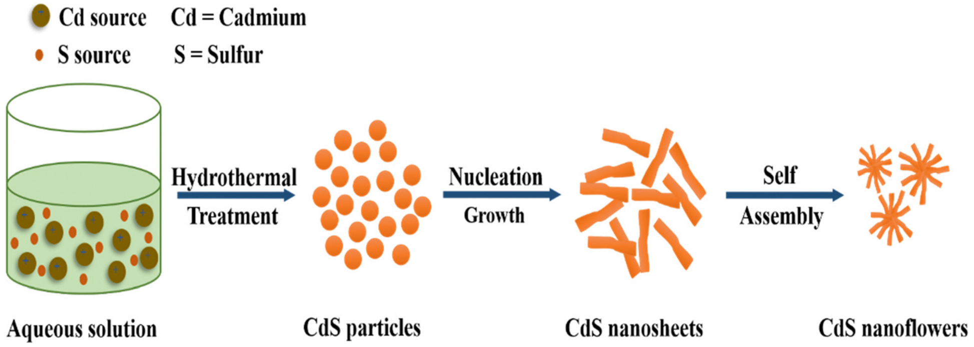

Fig. 2 Exploring CdS nanoflower formation through the hydrothermal treatment technique.

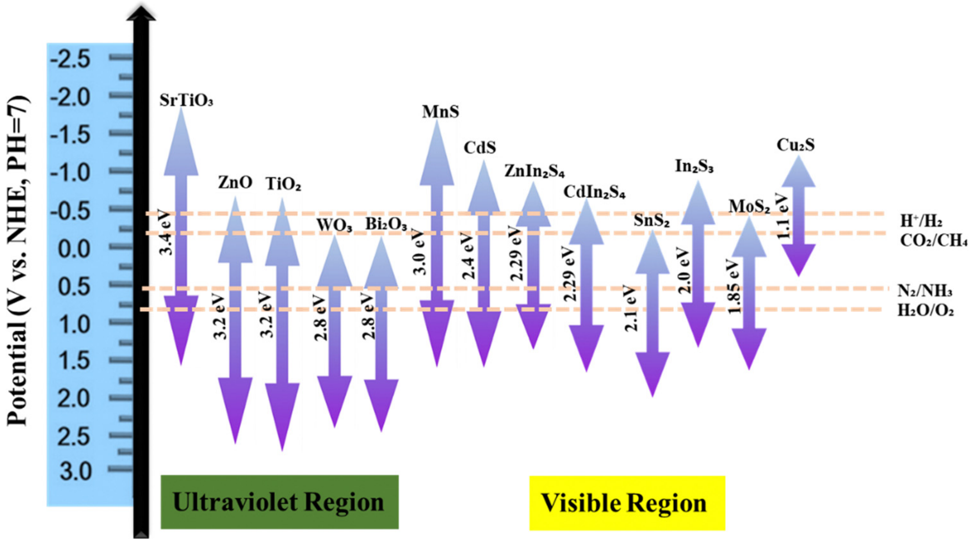

Fig. 3 Energy band gap values of key metal sulfide nanoparticles.

affecting metal sulfide-based dye degradation processes. To our best knowledge, this review is the first detailed report on the RMS regarding the synthesis of nanomaterials and their application in photocatalytic processes. This study will be the new horizon for the people working on the synthesis of such materials and their uses.

2. Metal sulfide nanoparticles

Metal sulfide nanoparticles refer to nanoscale particles composed of metal and sulfur atoms.[40,41] These nanoparticles exhibit unique optical, electrical, and chemical properties. Their small size and high surface area-to-volume ratio make them excellent candidates for catalytic reactions and energy storage applications.[42] Metal sulfides are of three main types: (a) pure metal sulfides, (b) doped metal sulfides, and (c) composite metal sulfides.

Those purely composed of a single metal exhibit catalytic, magnetic and electrochemical properties.[43,44] The structural, electrochemical, magnetic, photo-catalytic and catalytic properties of metal sulfides can be enhanced, when doped metal chalcogenides are used.[45] In this process, binary metals are used, with one present in high concentration and other in a small concentration.[46] Different metals like Ce, Sr, Cu, Co, *etc.* can be used as a dopant. A metal sulfide nanocomposite refers to a material composed of two or more distinct components, with one of the components being a metal sulfide.[47]

3. Synthetic approaches for metal sulfide nanoparticles

Two common methods for synthesizing metallic nanoparticles are top–down and bottom–up approaches. These methods differ primarily in the type of precursor used for nanoparticle preparation.[48] The top–down approach employs bulk materials as precursors,[49] while the bottom–up approach utilizes atoms or molecules.[50] Understanding these differences is essential for tailoring nanoparticle synthesis and properties for specific applications. Fig. 4 represents the synthetic approaches for metal sulfide nanoparticles.

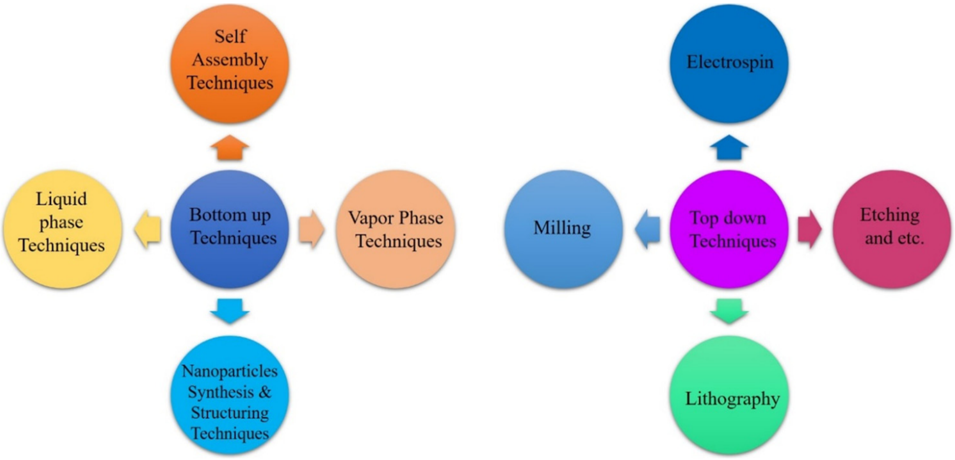

Fig. 4 Systematic techniques for the synthesis of metal sulfide nanoparticles.

3.1. Top–down method

The preparation of small nanosized particles involves the breakdown of bulk precursor material using various physical methods, such as sputtering, grinding, milling, thermal or laser ablation.[51–55] These processes result in the formation of nanoparticles with reduced dimensions compared to the original bulk material.[56] Top–down methods are categorized into two type of methods:

Scotch tape method. In this method, there is no chemical reaction involved and it is therefore called a non-destructive method.[57] This is a simple process that results in the production of nanoflake-like particles.[58]

Physical method. Various physical methods like mechanical milling,[59] ultra-sonication or liquid phase exfoliation[60] and electron spray pyrolysis[61] are used.

3.1.1. Mechanical milling. It is an inexpensive method for producing NPs from bulk and kinetic energy is transferred from the grinding medium to the material during reduction.[62] Reduction in particle size with high energy ball mining is the working principle involved in this method (Fig. 5).[63] NPs are produced by adding bulk powder and heavy balls that rotate at high speed in a container, resulting in the production of small size particles. Meng *et al.* (2021) reported the synthesis and optimization of a photocatalyst with a high-efficiency MoS_2 modification; this catalyst was composed of metal-free graphitic carbon nitride (g-C_3N_4), black phosphorus (BP), and MoS_2 (MCN/BP/MS). The optimized MCN/BP/MS photocatalyst exhibited excellent performance in hydrogen evolution, with a degradation rate of 100% in 25 min.[64]

3.1.2. Liquid-phase exfoliation. Exfoliation methods are efficient, low cost, result in fewer by-products and are convenient.[58] It is also one of the top–down methods in which solvent is scattered with a bulk of material. By means of mechanical processing techniques, such as ultra-sonication, 2D flake-like particles are generated through the exfoliation of the material. DMF is used as a solvent in this method. This approach is used for the fabrication of monolayer nanosheets with a thickness of <1 nm.[65] Hadi *et al.* (2018) explored a new method to increase the output of liquid-phase exfoliation of graphite to graphene sheets. The technique involves utilizing magnetic Fe_3O_4 nanoparticles as a "particle wedge" to aid in delaminating graphitic layers (Fig. 6). The use of Fe_3O_4 particles and ultrasonic waves generates strong shear forces, leading to improved exfoliation of graphite. This approach provides high-quality graphene sheets, and the separation of Fe_3O_4 particles from the graphene solution is easily accomplished due to the magnetic properties of Fe_3O_4 nanoparticles.[66]

3.1.3. Electrospray pyrolysis. This method involves the delivery of precursors in the gaseous form into a heated

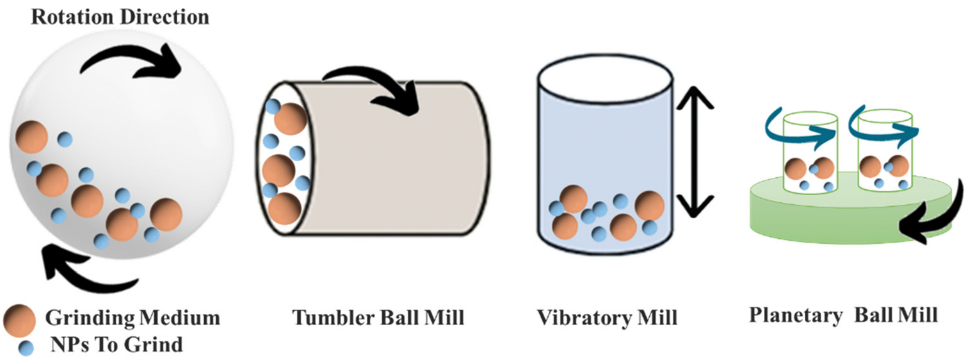

Fig. 5 Different mechanisms for mechanical ball milling.

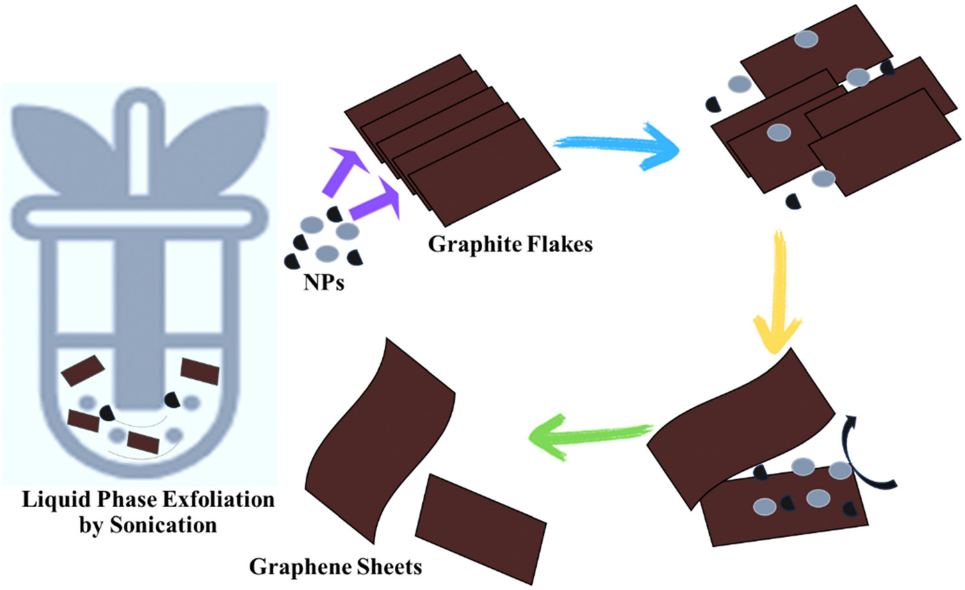
NPs
Graphite Flakes
Liquid Phase Exfoliation by Sonication
Graphene Sheets

Fig. 6 Nanomaterials for delaminating graphitic layers *via* the liquid phase exfoliation method.

reactor.[67] The precursor is facilitated using a nebulizer system, which comprises a fluid nebulizer, a vertical tubular reactor, and a precipitator.[56] Lee *et al.* (2021) studied Au/ZnO to control the electron–hole recombination of the photocatalyst. The ultrasonic spray pyrolysis method was employed to generate Au/ZnO particles under different conditions (Fig. 7). The photocatalytic decomposition rate of rhodamine-B was faster than that of ZnO in all Au/ZnO particles, with the best photocatalytic performance observed in particles containing 0.1 mass% Au supported on ZnO. Additionally, optimal photolysis activity occurred when 10 mg of Au/ZnO particles was added to 100 mL of a 5 mg L^{-1} RhB aqueous solution.[68]

3.2. Bottom–up method

In this approach, small particles, such as atoms or molecules, are merged to prepare nanoparticles (NPs). NPs are synthesized using chemical and biological techniques.[69] Fig. 8 illustrates the general mechanism of bottom–up and top–down approaches for metal sulfide nanoparticles.

3.2.1. Chemical methods for nanoparticle synthesis. Chemical methods are superior in terms of the rate of production and the production of nanoparticles with specific and controllable sizes. Metallic precursors, stabilizing agents and reducing agents are mainly used in chemical methods.[70]

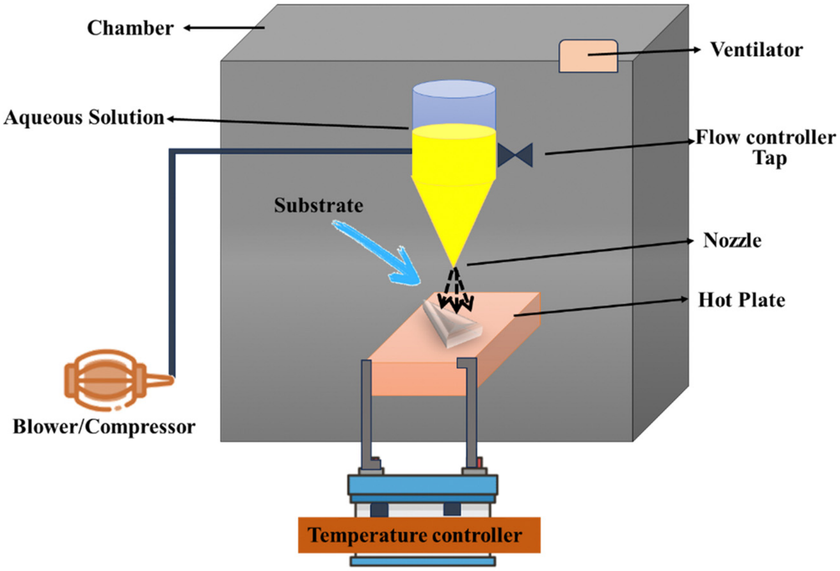
Chamber
Ventilator
Aqueous Solution
Flow controller Tap
Substrate
Nozzle
Hot Plate
Blower/Compressor
Temperature controller

Fig. 7 A complete setup for electrospray pyrolysis.

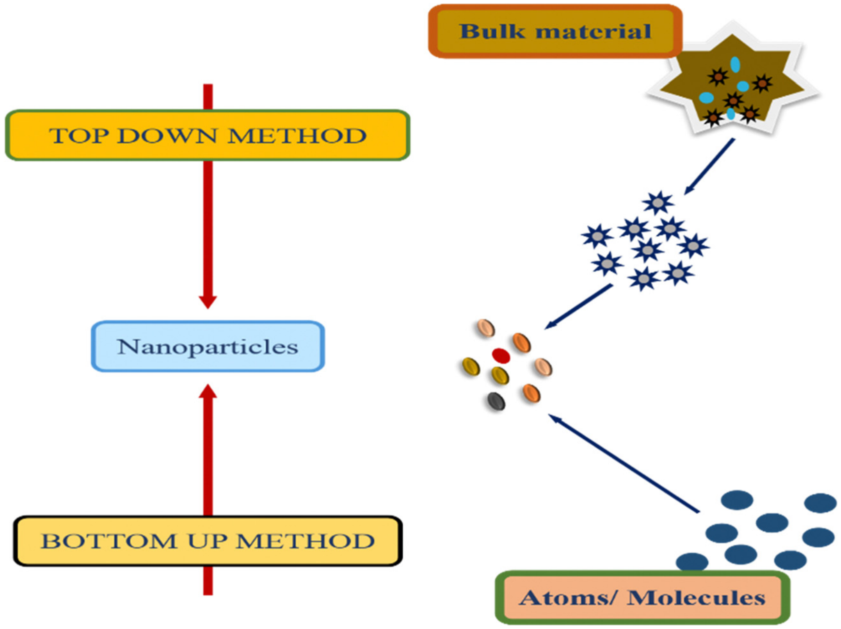

Fig. 8 General mechanism of bottom–up and top–down approaches.

Hydrothermal method. The synthesis of metal sulphides through the hydrothermal method needs a closed system with regulated temperature and pressure.[71] This is a low cost method for the synthesis of MoS_2 NPs. Sodium molybdate is used as the Mo precursor while thiourea and thioacetamide are used as sulphur sources.[72] This eco-friendly approach eliminates the need for pH control and complexing agents. Through this method, FeS_2,[73] CuS,[74] Ag_2S,[75] MoS_2[76] and CdS[77] are prepared. NPs are synthesized by heating a mixture of metal salts and sulfide sources. The commonly used metal sources include chlorides or nitrates, while organic sulfides serve as sulfide sources. This technique primarily generates nanoparticles in an autoclave. The synthesis of Ag_2S nanoflowers *via* hydrothermal treatment methodology is depicted in Fig. 9.

Amral *et al.* (2022) synthesized MoS_2 nanoflower-like nanoparticles by setting the autoclave temperature at 180 °C for 20 hours and utilizing molybdenum oxide and potassium thiocyanate as precursors. Temperature and duration have a significant influence nanoparticle architecture, with coral-like structures observed at 150 °C for 25 hours and nanosheet structures with extensive surface areas obtained at 240 °C for 47 hours.[58] Wang *et al.* (2023) prepared ZnS/TiO_2 heterojunction photocatalysts by hydrothermally depositing ZnS nanoparticles on TiO_2 nanofibers. Fig. 10 illustrates the synthesis of MoS_2 nanoflowers by using a hydrothermal method.

Microwave-assisted method. In this approach, there is an interplay between the material and microwaves, transmitting heat energy from the exterior to the interior, resulting in a thermal response. Internal heat generation within the reaction chamber, rather than external induction, is observed (Fig. 11). Microwave reactors offer a safer, greener alternative to conventional oil bath heating.[78] Thermally decomposing metal acetates produce PbS[79] and CdS nanoparticles.[80] Iravani *et al.* (2014) synthesized CdS through a preparation method that involves dissolving cadmium acetate and thiourea in ethylene glycol, adding NaOH as a capping agent, and evaporating the solvent through microwave irradiation. The resulting NPs are collected after cooling, washing, and drying.[81]

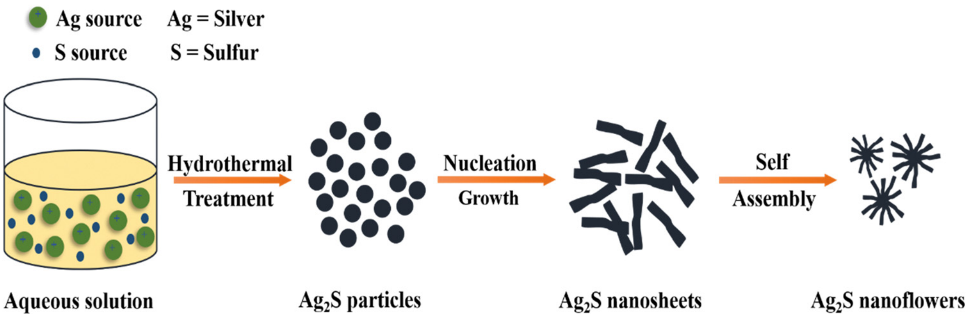

Fig. 9 Synthetic representation of Ag_2S nanoflowers by the hydrothermal method.

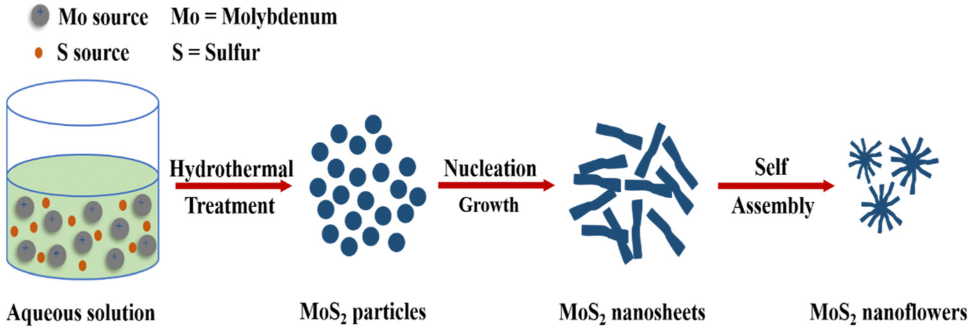
Mo source Mo = Molybdenum
S source S = Sulfur
Hydrothermal Treatment
Nucleation Growth
Self Assembly
Aqueous solution
MoS2 particles
MoS2 nanosheets
MoS2 nanoflowers

Fig. 10 Systematic representation of hydrothermal technique for the synthesis of MoS_2 nanoflowers.

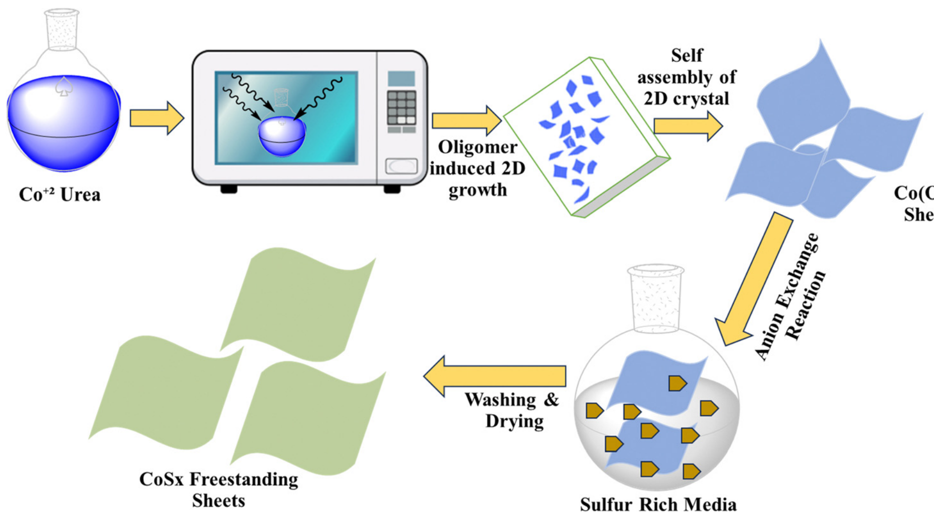
Co+2 Urea
Oligomer induced 2D growth
Self assembly of 2D crystal
Co(OH)2 Sheets
Anion Exchange Reaction
Sulfur Rich Media
Washing & Drying
CoSx Freestanding Sheets

Fig. 11 Synthesis of CoSx using a microwave-assisted approach.

Solvothermal method. In this procedure, metal sulfide nanoparticles are synthesized within a sealed system, involving chemical reactions between precursors in a solvent environment.[41,71] This technique necessitates the use of solvents in precursor reactions, with DMF and water being the primary choices for this purpose. The key factors influencing reaction control and product size include temperature, solvent, duration, and precursors.[82] The solvothermal approach, a simple technique for synthesizing NPs with various shapes, is employed to produce MoS_2/rGO NPs. This cost-effective method, featuring a brief processing time, is ideal for creating metal sulfides with minimal crystallite size. Sambathkumar *et al.* (2021) studied the Bi[DTC]$_3$ complex and hexadecylamine (HDA), which were combined in a 1 : 1 weight ratio and dispersed in 100 mL of dimethylformamide (DMF). The Bi_2S_3 product was collected, dried overnight in an oven at 60 °C, and analyzed using various analytical techniques (Fig. 12).[83]

Precipitation method. This is a simple synthetic method for the preparation of metal sulphide NPs and does not need extreme conditions. In_2S_3 has been synthesized by this method using $Na_2S{\cdot}3H_2O$ as a precipitating agent.[84] Afsheen *et al.* (2020) prepared CuS nanoparticles (NPs) through a method that employed Na_2S as the sulfur donor and $Cu(OAc)_2$ as the metallic precursor. Various metal sulfide NPs, such as AgS,[85] PbS,[86] Bi_2S,[87] and Au/Ag_2S,[88] were generated using this approach. For the preparation of Ag_2S, $AgNO_3$ was dissolved in toluene and oleyamine, with stirring for 60 min at room temperature, resulting in the formation of Ag_2S NPs.[10]

Chemical vapour deposition method. In this approach, film generation occurs *via* the deposition of gaseous molecules through chemical reactions, which is essential for film creation. Film growth in CVD systems relies on substrate characteristics and surface processing (Fig. 13).[89] A number of methods are used for depositions, including photo-initiated chemical vapour deposition,[90] plasma enhanced chemical vapour deposition[91] and thermally active chemical vapour deposition method.[92] In the CVD technique, precursors amass to create nanosheets, generating a significant nanoparticle yield at minimal cost. High-purity materials are deposited, and CVD necessitates a lower vacuum than PVD methods.[93] CVD is a very effective approach for the preparation of monolayer transition metal chalcogenides.[94]

3.2.2. Biosynthesis approach.

Biosynthesis of metal sulfides by bacteria, fungi, algae and actinomycetes has garnered immense attention in the field of nanotechnology.[95] Bacteria possess the

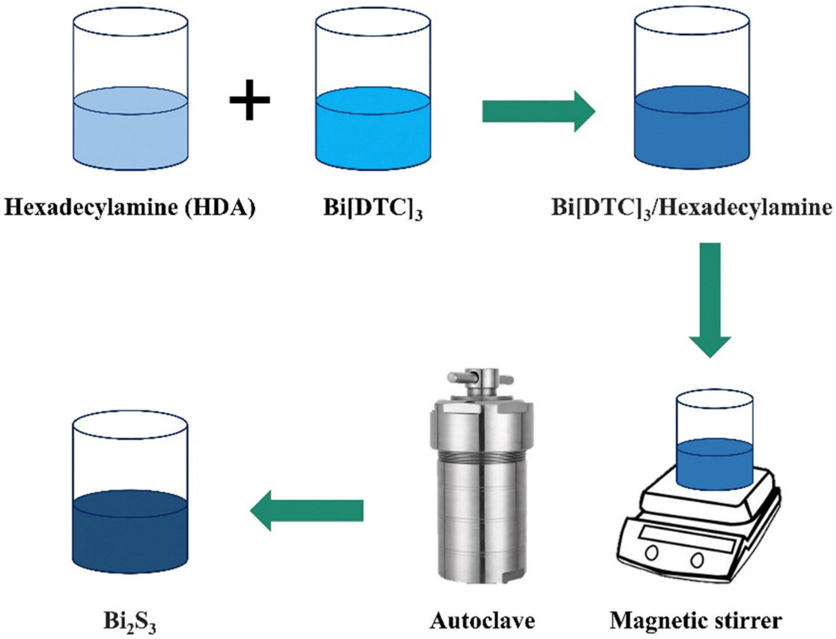
Hexadecylamine (HDA)
+
Bi[DTC]$_3$
Bi[DTC]$_3$/Hexadecylamine
Magnetic stirrer
Autoclave
Bi$_2$S$_3$

Fig. 12 Synthesis of Bi_2S_3 by a solvothermal method.

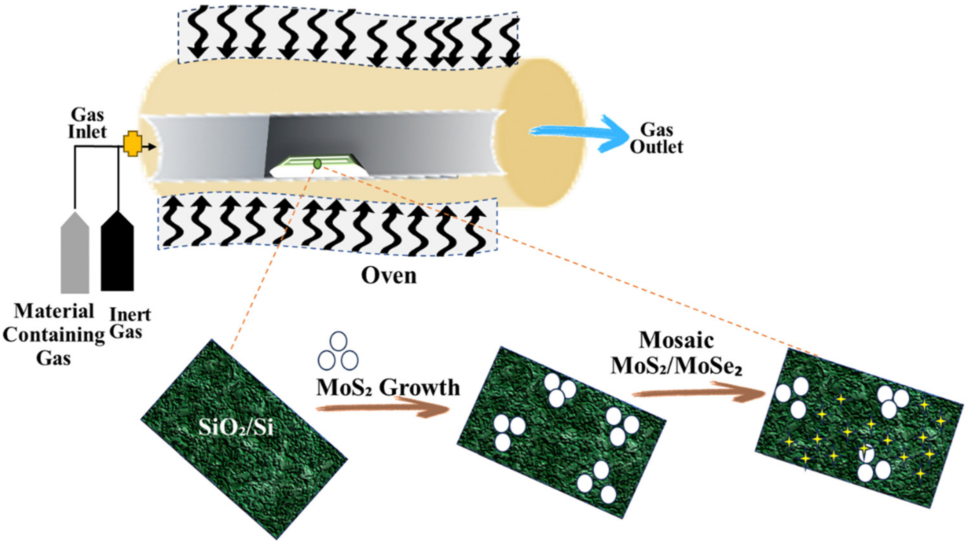
Gas Inlet
Gas Outlet
Oven
Material Containing Gas
Inert Gas
SiO₂/Si
MoS₂ Growth
Mosaic MoS₂/MoSe₂

Fig. 13 Synthesis of $MoS_2/MoSe_2$ by chemical vapor deposition.

capability to reduce metallic ions into nanoparticles and are one of the most suitable candidates for metal sulfide nanoparticles because of their manageable nature and high growth rate. Metal complexation typically involves bacterial cell wall functional groups like hydroxyl, amine, and carbonyl groups.[71] Fungal synthesis presents challenges compared to bacterial methods due to difficulties in manipulation and increased intracellular absorption.[96] However, fungi exhibit superior productivity and metal tolerance.[97] Economical and efficient nanoparticle production (Fig. 14), such as CdS[98] and ZnS,[99] is achievable through *Fusarium oxysporum's* extracellular process, owing to its enhanced bioaccumulation of metal ions.[69] Recent studies reveal that besides fungi, yeast is utilized for biogenic synthesis due to its innate ability to assimilate toxic metal ions from the environment. Yeast cells can adapt to metal toxicity through detoxification processes. A marine ascomycetous yeast, *Yarrowia lipolytica*, produces silver nanoparticles.[100] The advantages and disadvantages of the different methods have been listed in Table 1. The various properties of metal sulfide nanoparticles have been listed in Table 2.

4. Synthetic parameters of metal sulfide nanoparticles

Metal sulfide nanoparticles refer to nanoscale particles composed of metal and sulfur atoms.[40] These nanoparticles

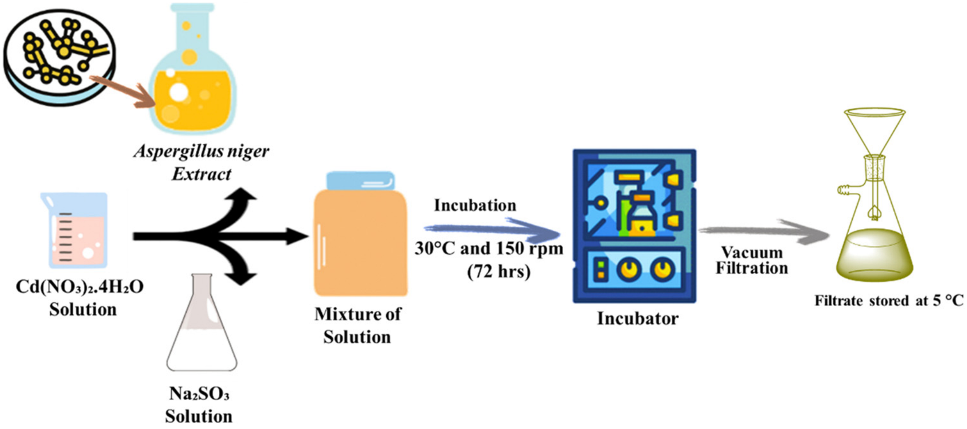

Fig. 14 Synthesis of CdS NPs using the extract of *Aspergillus niger*.

Table 1 Advantages and disadvantages of different nanoparticle synthesis methods

Method	Advantages	Disadvantages	Ref.
Mechanical milling	Scalable and relatively simple process Suitable for brittle materials	High energy consumption Potential contamination from milling media	56
Liquid phase exfoliation	Scalable and versatile Suitable for 2D materials	Yield can vary depending on material May require surfactants for stability	101
Electro spray pyrolysis	Precise control over particle size High uniformity	Complex equipment and operation Limited to certain materials	102
Hydrothermal method	Mild conditions Narrow size distribution	Limited to certain compositions Long processing times	103
Microwave assisted method	Rapid heating and synthesis Enhanced reaction rates	Limited to specific materials Potential hotspots and uneven heating	104
Solvothermal method	High purity and crystallinity Controlled morphology	High pressure and temperature required Long synthesis times	105
Precipitation method	Simple and cost-effective Suitable for bulk production	Limited control over particle size May require additional purification	106
Chemical vapor deposition	Precise control over film thickness High purity and uniformity	Complex setup and operation Limited to thin films	107
Biosynthesis approach	Environmentally friendly Biocompatible nanoparticles	Variable product quality Limited scalability	108

exhibit unique optical, electrical, and chemical properties.[117] Huerta *et al.* (2018) synthesized PVP capped CdS nanoparticles *via* hydrothermal method. The synthesized nanoparticles exhibit flower-like morphology.[1] Table 3 presents synthetic characteristics of metal sulfide nanoparticles.

5. Photo catalysis mechanisms: understanding the science behind the light-driven reactions

Photocatalysis is a promising green technology that harnesses the power of light to drive chemical reactions typically by employing semiconductor materials as photocatalysts to convert solar energy into chemical energy.[208] This process has gained considerable attention in recent years due to its potential applications in various fields, such as environmental remediation, energy production, and organic synthesis. The photocatalytic removal of pollutants possesses several advantages[209,210] including utilization of renewable resources (such as sunlight), a simple operation scheme, efficient removal and the complete mineralization of dyes, *etc.*[170] Organic dyes not only damage the aesthetical aspects of water but are also inappropriate for the ecosystem; they can damage the irrigational land, pose health hazards, and disturb the food chain.

Photocatalysis serves as a remarkable solution for various environmental challenges.[14,211] The conventional semiconductors employed as photocatalysts include ZnO,[212,213] TiO_2,[214,215] CdS,[216,217] *etc.*, which play a significant role in the degradation of environmental contaminants. Photocatalysis is a cost-effective, fast and straightforward method for the cleansing of organic and inorganic contaminants from wastewater.[165] In photocatalytic degradation, the commonly involved active species are electrons, holes, hydroxyl ($^{\bullet}OH$) and superoxide ($O_2^{\bullet-}$) radicals. Metal oxides have confined 2p orbitals for oxygen due to the high effective mass of hole carriers. In contrast, metal sulfides exhibit 3p orbitals with a smaller band gap and a greater capacity to capture visible light and facilitate charge transfer. However, a higher recombination rate of electron–hole pairs may impede photocatalysis.[176] The unique properties of semiconductor materials make them particularly interesting for photocatalytic reactions for

Table 2 Comparative analysis of metal sulfide properties

Metal sulfide	Crystal structure	Color	Melting point (°C)	Band gap (eV)	Electrical conductivity	Solubility	Ref.
FeS_2	Cubic	Pale yellow	1065	0.95–1.2	Semiconductor	Insoluble	109
PbS	Cubic	Gray	1123	0.36	Poor conductor	Insoluble	10
HgS	Hexagonal	Red	580	~1.6	Insulator	Insoluble	110
Cu_2S	Monoclinic	Gray-black	1035	~0.9	Semiconductor	Insoluble	111
Sb_2S_3	Orthorhombic	Gray	550	~1.1	Poor conductor	Slightly soluble	112
CuS	Hexagonal	Indigo blue	~500	~1.5	Semiconductor	Insoluble	113
ZnS	Hexagonal	White	1182	3.5–3.8	Semiconductor	Insoluble	114
NiS	Hexagonal	Greenish	~797	~1.3	Semiconductor	Slightly soluble	115
MoS_2	Hexagonal	Dark gray	1850	~1.2	Semiconductor	Insoluble	116

environmental applications.[172] Fig. 15 illustrates advanced TiO_2-based photocatalytic systems for methylene blue degradation.

Although photocatalysis is an effective technology but photocatalyst materials have some issues, such as the bandgap of catalysts, source of light, nature of dye, the concentration of dye and some other factors that may limit the photocatalytic action of photocatalysts.[167] Methylene blue (MB) dye is a common industrial pollutant that poses serious environmental and health risks when released into water bodies. Fig. 16 illustrates the photocatalytic degradation mechanism of MB dye using liquid chromatography–mass spectrometry (LC-MS) to identify the intermediates and products formed during the process.[31]

5.1. Photocatalytic degradation of methylene blue (MB) using NiS

In the photocatalytic degradation of MB using a UV-visible spectrophotometer, the $\lambda_{\max}$ of 10 mg L^{-1} of MB dye was observed at 670 nm.[151] Visible light photons with energy equal to or exceeding the bandgap excite the photocatalyst valence band electrons, initiating redox reactions. Photogenerated electrons on the photocatalyst surface create superoxide radicals by reacting with oxygen, while photogenerated holes generate hydroxyl radicals through water interaction.[14] The photocatalyst absorbs photons from the irradiation source, which lights the sample solution. This absorption excites semiconductor electrons from the valence band to the conduction band. The photocatalyst generates electron–hole pairs from electron excitation. Positively charged holes form in the valence band and electrons are promoted to the conduction band, forming mobile charge carriers. These photogenerated electrons and holes react. Electrons form oxygen radicals ($O_2^{\bullet-}$) and hydroxyl radicals ($^{\bullet}OH$) from oxygen molecules in the environment, while holes generate positively charged holes. The degradation process uses sample solution water molecules as intermediates. Electrons from the conduction band react with oxygen to make oxygen radicals, which react with water molecules to form hydroxyl radicals and protons. Hydroxyl ions (OH^-) in the solution combine with water molecules to create hydrogen peroxide. This reactive species can participate in degradation activities as a powerful oxidant. Hydrogen peroxide from the preceding step can interact with oxygen radicals to produce $^{\bullet}OH$ and hydroxyl ions. These very reactive hydroxyl radicals degrade organic substances, including colours. In one situation, hydroxyl radicals immediately react with dye molecules, starting degradation pathways that break down the colour into safer components. Alternatively, hydroxyl radicals might adsorb and degrade dye molecules on the photocatalyst. Parallel to the valence band, positively charged holes (h^+) can combine with hydroxyl ions to form hydroxyl radicals ($^{\bullet}OH$). These hydroxyl radicals may degrade dye molecules or engage in oxidation events. The mechanism for the degradation of methylene blue is shown in Fig. 17.

5.2. Photocatalytic degradation of crystal violet using Nis

The degradation of CV (crystal violet) dye at various degradation times and catalyst doses (5–30 mg) was observed under sunlight irradiation followed by, magnetic stirring. The photocatalytic breakdown of crystal violet dye includes photo-induced processes assisted by the photoactive catalyst. The photocatalyst absorbs irradiation. This energy absorption causes an electron to shift from the photocatalyst's valence band (VB) to its conduction band (CB). An electron moves from the VB to the photocatalyst CB after energy absorption. This produces a h+ in the VB and an e− in the CB. The excited electron interacts with ambient molecular oxygen (O_2) in the CB. This interaction generates superoxide radicals. These extremely reactive superoxide radicals have oxidative potential. In the photo catalyst's VB, H_2O adsorbed on the surface is oxidized. Hydrogen ions and hydroxyl radicals ($^{\bullet}OH$) result from this oxidation. Strong oxidizers are hydroxyl radicals. VB hydroxyl radicals ($^{\bullet}OH$) and CB superoxide radicals ($O_2^{\bullet-}$) react with water and color molecules. These reactions produce water and CO_2 as intermediates. The crystal violet dye molecules adsorbed on the photocatalyst interact with radical production and electron transfer intermediary species. These interactions degrade dye molecules into nontoxic components. Photocatalytic degradation of crystal violet dye uses photon energy to trigger electron transfers, reactive radical production, and dye molecule chemical processes. The dye degrades into water and carbon dioxide. The mechanistic aspects of this photodegradation are given in Fig. 18.[152]

5.3. Photocatalytic degradation of rhodamine B dye using NiS

The catalyst molecule may directly interact with the dye molecule and actively participate in the photocatalytic dye degradation. Also, the standard redox potential of $OH^-/^{\bullet}OH$ (+1.9 V *vs.* NHE) was found to be less positive than the valence band

Table 3 Key synthetic parameters and physicochemical properties of metal sulfide nanoparticles

Sr. no.	Metal sulfide NPs	Method	Metal precursor	Morphology	Size (nm)	Ref.
01.	PVP capped-CdS	Hydrothermal	$Cd(NO_3)_2{\cdot}4H_2O$, CH_4N_2S	Flower-like	—	1
02.	CdS/Ag	Hydrothermal	$Cd(O_2CCH_3)_2(H_2O)_2$, $AgNO_3$	Spherical	28.3	118
03.	CdS-Ag_2S	Co-precipitation	$CdCl_2$, $Na_2S_2O_3$	—	—	119
04.	ODA-CdS	Hydrothermal & chemical	$Cd(S_2CNR_2)_2$	Sphere	1.92–5	120
05.	CdS/PVA	Precipitation deposition	CdAc	Nematic	4–8	121
06.	CdS	Hydrothermal	$Cd(NO_3)_2{\cdot}4H_2O$, $Na_2S{\cdot}9H_2O$	Hexagonal	—	122
07.	CuS–TiO_2	Photochemical	$CuSO_4$,$Na_2S_2O_3$	—	2.75 ± 0.8	123
08.	Cu_2SnS_3	Hydrothermal	$H_2N–CH(SH)–CH_2–COOH$	Pin-like	~40	27
09.	CuS	—	$Cu(C_5H_{10}NS_2)_2$	Hexagonal covellite	31.47	124
10.	CuS-QDs/ZnO	Hydrothermal	$Cu(CH_3COO)_2$	Sphere like	4	125
11.	CdS/ZnO	Deposition	$C_4H_6O_2Cd.H_2O$	Hexagonal crystal	400–200	126
12.	Ge–Ce–CuS	Hydrothermal	$Cu(C_2H_3O_2)_2{\cdot}H_2O$, $Ce(NH_4)_2(NO_3)_6$	Hexagonal	100–200	127
13.	Ni-Cd-S/rGO	Hydrothermal	$Cd(NO_3)_2$, $Ni(NO_3)_2{\cdot}6H_2O$	Cauliflower	18 nm	128
14.	CdS	Hydrothermal	C_2H_5NS, $Cd(NO_3)_2{\cdot}5H_2O$	Hexagonal	66.28 ± 12.95	129
15.	CdS	Mechanochemical	$Cd(CH_3COO)_2$, Na_2S	Hexagonal	10	130
16.	CuS	Solvothermal	$CuCl_2$,CH_4N_2S	Spherical	10–12	131
17.	CNT/CuS	Coprecipitation	$Cu(NO_3)_2$	Flake like & tubular	10–25	132
18.	CuS/In_2S_3	Solvothermal	$Cu(C_5H_7O_2)_2$	—	6.34 ± 0.31	78
19.	CdS	Green synthesis	$CdCl_2$,Na_2S	Hexagonal	50–180	133
20.	CdS	Hydrothermal	$CdCl_2$	Nanopetals		134
21.	ZnFe/CuS	Hydrothermal	$CuSO_4{\cdot}5H_2O$, $Fe(NO_3){\cdot}9H_2O$	Cubic shaped	26–64	135
22.	CdS	Hydrothermal	$Cd(NO_3)_2{\cdot}4H_2O$, $Na_2S{\cdot}9H_2O$	Hexagonal	500	136
23.	RE-CdS	—	$CdCl_2$	Wurtzite	10 ± 2	137
24.	CdS/SnO_2	Hydrothermal & co-precipitation	$Cd(NO_3)_2$, Na_2S	—	18	138
25.	CdS/TiO_2	Melt quench	—	Stone-like	5.33	139
26.	CdS/g-C_3N_4/MOF	Solvothermal	DMF, $Cd(CH_3COO)_2{\cdot}2H_2O$, CH_4N_2S	—	—	140
27.	CdS/ZnO	Hydrothermal	ZnO, $Cd(CH_3COO)_2{\cdot}2H_2O$	Spherical	71.09 ± 16.66	141
28.	CdS/ZnO	Hydrothermal	$Zn(OAC)_2{\cdot}2H_2O$	—	—	142
29.	CdS/BiOBr	Precipitation	$Cd(NO_3)_2{\cdot}2H_2O$	Rod like	400	143
30.	Fe/CdS	Chemical precipitation	$CdCl_2{\cdot}5H_2O$, $Na_2S{\cdot}5H_2O$, $Fe(NO_3)_3{\cdot}9H_2O$	Spherical	11.6–4.1	144
31.	BiOCl-Au/CdS	Chemical bath deposition	$HAuCl_4$, NH_2CSNH_2, $Cd\ (CH_3COOH)_2$	—	1000	145
32.	ZnO/CdS/CuS	—	$Cu(NO_3)_2.3H_2O$, CH_4N_2S	—	10–15	146
33.	CuS	—	CH_4N_2S, $Cu(C1_2H_25SO_4)(OH)_2$	Hexagonal covellite	~10	147
34.	NiS_2	Co-precipitation	$Ni(dtc)_2$, $C_2H_4(NH_2)_2$	Spherical	62	148
35.	NiS_2	Wet impregnation ultrasonic assisted	$H_{12}N_2NiO_{12}$, C_2H_5NS	Crystalline	30.47	149
36.	NiS_2	Co-precipitation	$[Ni(dtc)_2]$, $C_6H_{18}N_4$	Orthorhombic	5–200	150
37.	NiS_2	Hydrothermal	$Ni(NO_3)_2{\cdot}6H_2O$	Cubic crystalline	22	1
38.	NiS_2	Chemical precipitation	$NiSO_4$,Na_2S	Hexagonal	0.26	151
39.	NiS_2	Hydrothermal	$NiCl_2{\cdot}6H_2O$, $C_3H_7NO_2S$	Crystalline	9.5	14
40.	NiS_2	Coprecipitation	$NiCl_2{\cdot}6H_2O$, Na_2S	Cubic crystalline	22.11	152
41.	NiS_2	Hydrothermal	$NiSO_4$	Spherical crystalline	12.1	153
42.	NiS_2	Solution combustion	$(Ni(NO_3)_2{\cdot}6H_2O)$, $(CS(NH_2)_2)$	Spherical	200–300	154
43.	NiS_2	Hypothermal	$Ni(NO_3)2{\cdot}6H_2O$, $SC(NH_2)_2$	Rhombohedral	0.25	155
44.	NiS_2	Wet chemical	$(NiCl_2.6H_2O)$	Crystalline	51	156
45.	NiS_2	Solvothermal	C_3N_4/Ni-MOF	Spherical	0.24–0.55	157
46.	NiS_2	Hydrothermal	$NiCl_2{\cdot}6H_2O$	Plane crystal	200	158
47.	NiS_2	Solution combustion	$Ni(NO_3)_2{\cdot}6H_2O$	Sponge crystalline	100–200	159
48.	CoS_2	Precipitation	$C_4H_6CoO_4{\cdot}4H_2O$	Hexagonal	24.37	17
49.	CoS_2	Solvothermal	$CoH_{12}N_2O_{12}$	Crystalline	33.97	160
50.	$NiCo_2S_4$	Precipitation	$Ni_2N_2O_6{\cdot}6H_2O$, $CoN_2O_6{\cdot}6H_2O$	Spherical	500	161
51.	CoS_2	Precipitation	$[Ni(S_2CNMe_2)(C_5H_4FeC_5H_4)$-$(C_2H_5C_6H_5)]_2$	Spherical and ring	20	162
52.	CoS_2	Precipitation	$[Ni(S_2CNMe_2)(C_5H_4FeC_5H_4)$-$(C_2H_5C_6H_5)]_2$	Spherical	15–20	163
53.	Co_5S_2	Reverse emulsion	$Co\ (NO_3)_2{\cdots}6H_2O$	Cubic	230	164
54.	NiS_2-rGO	Hydrothermal	$NiCl_2$	Plane crystalline	0.20	13
55.	CoS_2	Electrochemical deposition	Na_2S	Nanocrystalline	14	165
56.	Co_9S_8	Solvothermal	$CoSO_4{\cdot}7H_2O$	Flower-like crystalline	230	166
57.	Co-ZnS	Chemical-precipitation	$Zn(CH_3COO)_2{\cdot}2H_2O$, $Co(NO_3)_2{\cdot}6H_2O$	Spherical particles	3.832	167

Table 3 (*continued*)

Sr. no.	Metal sulfide NPs	Method	Metal precursor	Morphology	Size (nm)	Ref.
58.	Ni–Co–S	Coprecipitation	$Co(CH_3COO)_2 \cdot 4H_2O$, $Ni(CH_3COO)_2 \cdot 4H_2O$	Crystalline	40–50	168
59.	NiS_2	Precipitation	$NiBr_2.3H_2O$	Rhombohedral	50	169
60.	NiS-In_2O_3/GO	Hydrothermal	In_2O_3 and NiS	—	66	170
61.	NiS-SiO_2	Ultrasound microwave	$Ni(CH_3CO_2)_2 \cdot 4H_2O$	Hexagonal crystalline	7.2	171
62.	CoS_2	Chemical precipitation	$Co(NO_3)_2 \cdot 6H_2O$	Flower-like crystalline	500	172
63.	NiS_2	Hydrothermal	$Ni(NO_3)_2 \cdot 6H_2O$	Crystalline	2–50	173
64.	NiS_2	Precipitation	$NiSO_4$	Powder	26.75	174
65.	Ni–Co–S	Precipitation	$Ni(OAc)_2.4H_2O$, $Co(OAc)_2.4H_2O$	Cubic crystalline	30–60	175
66.	CoS_2	Ultrasonication	$CoSO_4$ and Na_2S	Hexagonal plane	2.2	176
67.	$NaFeS_2$	Hydrothermal	$Na_2S.9H_2O$ & $Fe(NO_3)_3$	Monoclinic	25–30	177
68.	ZnS	Heating	$(ZnSo_4.H_2O)$, $C_2H_5NO_2$, $MnSO_4.H_2O$, Na_2S	Crystalline	—	178
69.	MoS_2-ZnS	Hydrothermal	MoS_2, ZnS film	Crystalline	20–25	179
70.	FeS_2	Hydrothermal	—	Nanostructures	—	180
71.	Cu_2SnS_3	Hydrothermal	—	—	—	181
72.	CoS/Ag_2WO_4	Chemical precipitation	—	—	—	182
73.	CdS	—	—	Hexagonal nanostructures	—	183
74.	NiS_2-rGO	Hydrothermal	—	Nanospheres	10 ± 0.317	184
75.	(CoS)	Precipitation	—	Nanostructure	—	185
76.	NiS/CNTs	Hydrothermal	—	—	—	186
77.	ZnS	Biomolecule-assisted	—	—	—	187
78.	CuS/CdS	Hydrothermal	—	—	—	188
79.	CuS/CuO	Thermal oxidation	—	—	—	189
80.	$CoFe_2O_4/MoS_2$	Hydrothermal	$Fe(NO_3)_3/Co(NO_3)_2$/PVP	Flower-like	—	190
81.	FeS_2	Hydrothermal	—	Crystalline	50	191
82.	pC/ZnS/CuS	Adsorption and deposition	—	—		192
83.	Fe_3O_4/CdS–ZnS	Brunauer–Emmett–Teller	—	Spherical shape	25–45	193
84.	ZnS QDs	Chemical precipitation	—	—	—	194
85.	ZnS/chitosan	Gelation		—	100	195
86.	CoS/Ag_2WO_4	Co-precipitation	$CoSO_4$ and Na_2S	Heterojunction	200	196
87.	ZnS-rGO	Solvothermal	—	Sphere	5–12	197
88.	CuS-ZnS-graphene	Hydrothermal	—	Spherical	5–20	198
89.	MoS_2	Hydrothermal	—	Crystalline	∼20–30	123
90.	Ag-ZnS	Sonochemically	—	Crystalline		199
91.	Mn-ZnS		—	Crystalline	1–10	200
92.	CuO-FeS_2	Hydrothermal	—	Heterostructure	—	201
93.	CTS + GO	Precipitation		Crystalline	—	202
94.	Sb_2S_3	Sol–gel	$SbCl_3$ and TAA	Spherical shape	∼180–500	203
95.	MoS_2/SnO_2	Hydrothermal	—	Heterostructure crystalline	12	204
96.	Bi_2S_3	One pot hydrothermal	—	Crystalline	—	205
97.	Ag-SnS	Hot injection	Ag and SnS	Nano crystalline	—	206
98.	Ag_2WO_4-MoS_2-GO	Hydrothermal	—	—	—	207

position of nickel sulfide.[156] The mechanism for the degradation of rhodamine is given in Fig. 19. Light absorption from an irradiation source propels the MoS_2/NiS_2 composite photocatalyst to degrade rhodamine B (RhB) dye through a series of complex stages. The MoS_2/NiS_2 composite photocatalyst absorbs photons, exciting electrons from the valence band to the conduction band. This excitation creates reactive species with high redox potential by generating electron–hole pairs. A multi-faceted cascade begins when photocatalyst conduction band electrons are activated. Water molecules near the conduction band electrons generate hydroxyl radicals ($^{\bullet}OH$) and hydrogen ions. Hydroxyl radicals are very reactive and break down organic dye molecules. Water and oxygen react in the photo catalyst's valence band to form hydrogen peroxide. The valence band holes facilitate hydrogen peroxide production in these processes. Additional reactive oxygen species promote decomposition. Hydroxyl radicals ($^{\bullet}OH$) from the conduction band and hydrogen peroxide (H_2O_2) from the valence band target rhodamine B dye synergistically. These reactive organisms break down dye molecules into simpler, ecologically friendly chemicals. The breakdown of RhB dye produces a mixture of compounds. Carbon dioxide, water, nitrate ions, and ammonium chloride are these products. These degradation products are quickly incorporated into the ecosystem and have no environmental effect.

5.4. Photocatalytic degradation of CR dye CoS-rGO

The hydrophobic nature of metal sulfide–rGO nanocomposites results in exceptional catalytic activity for water and organic pollutant decomposition. Sunlight exposure excites electrons in the valence band, causing them to move to the conduction band.[13] The CoSrGO (cobalt-sulfur reduced graphene oxide)

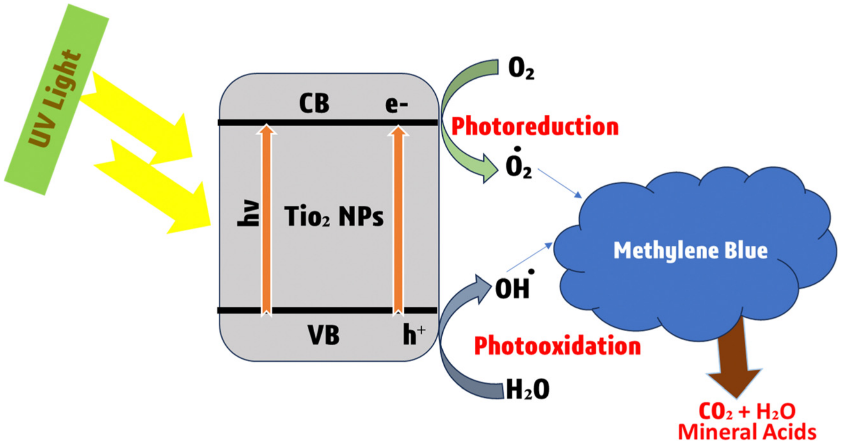
UV Light
CB
e-
hv
Tio₂ NPs
VB
h+
O₂
Photoreduction
Ȯ₂
Methylene Blue
OH˙
Photooxidation
H₂O
CO₂ + H₂O
Mineral Acids

Fig. 15 Representation of enhanced photocatalytic breakdown of methylene blue dye with TiO_2 nanoparticles.

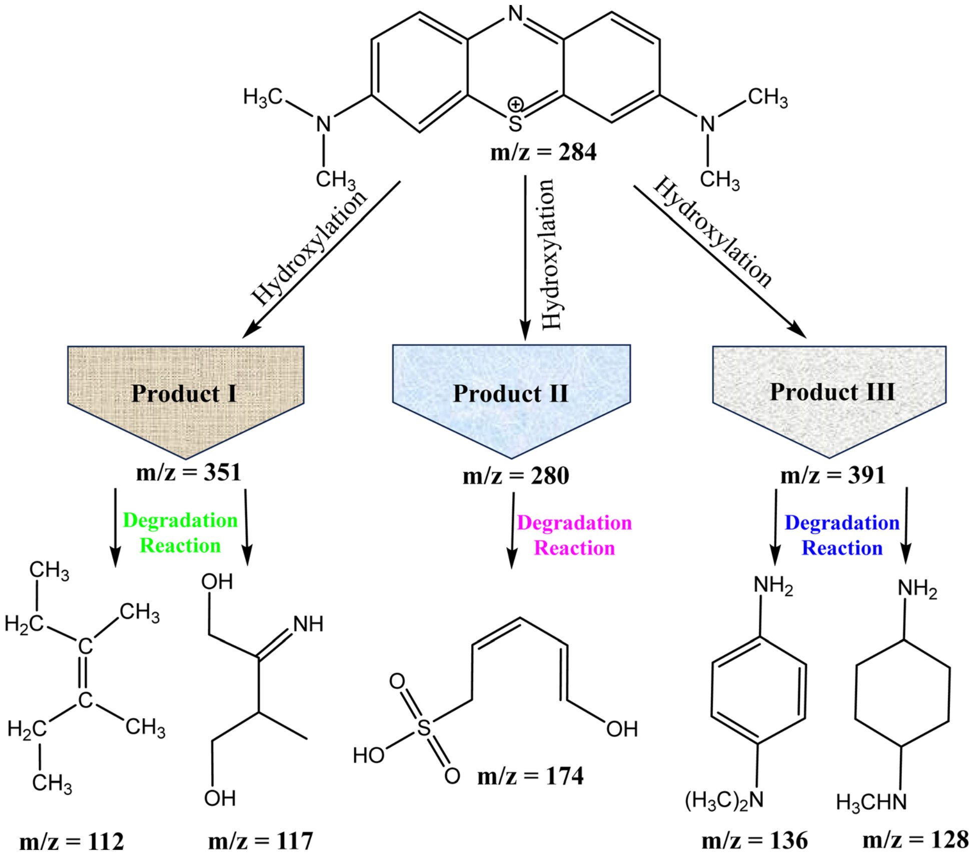
m/z = 284
Hydroxylation
Hydroxylation
Hydroxylation
Product I
Product II
Product III
m/z = 351
m/z = 280
m/z = 391
Degradation Reaction
Degradation Reaction
Degradation Reaction
m/z = 112
m/z = 117
m/z = 174
m/z = 136
m/z = 128

Fig. 16 Degradation pathway of MB dye from molecular breakdown to primary intermediates and the final product.

photocatalyst degrades CR (Congo red) dye molecules *via* light-induced reactions. Electrons in CoSrGO are excited by light from the irradiation source. Electrons move to the conduction band (CB) and leave holes in the valence band (VB) after this stimulation. The conduction band of CoSrGO reacts with environmental hydroxyl radicals (*OH). Reactive species that interact with CR dye molecules result from this process. The *OH radicals break the CR dye's molecular structure. In the valence band of CoSrGO, reduced graphene oxide (rGO) interacts with H_2O, O_2, and H^+ to collectively generate hydrogen peroxide. Hydrogen peroxide boosts the environment's oxidative potential, promoting the breakdown of organic molecules. In the valence band of CoSrGO, reduced graphene oxide (rGO) interacts with H_2O, O_2, and H^+ to collectively generate hydrogen peroxide. Hydrogen peroxide boosts the environment's oxidative potential, promoting organic molecule breakdown. Hydrogen peroxide (H_2O_2) reacts to form hydroxyl radicals (*OH). *OH radicals are potent oxidizers that

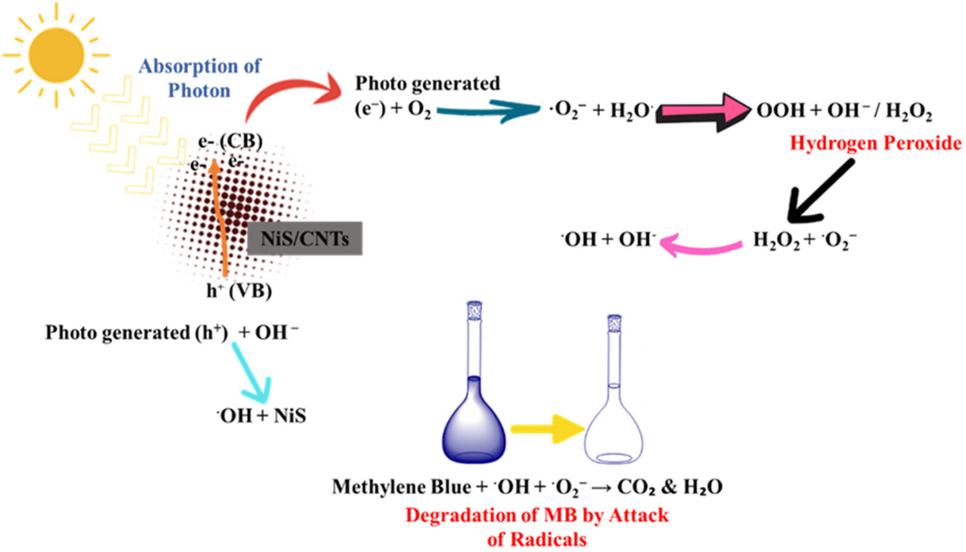
Absorption of Photon
Photo generated (e⁻) + O₂
·O₂⁻ + H₂O
OOH + OH⁻/ H₂O₂
Hydrogen Peroxide
e- (CB)
NiS/CNTs
h⁺ (VB)
·OH + OH⁻
H₂O₂ + ·O₂⁻
Photo generated (h⁺) + OH⁻
·OH + NiS
Methylene Blue + ·OH + ·O₂⁻ → CO₂ & H₂O
Degradation of MB by Attack of Radicals

Fig. 17 Mechanism of photocatalytic degradation of methylene blue (MB) using NiS.

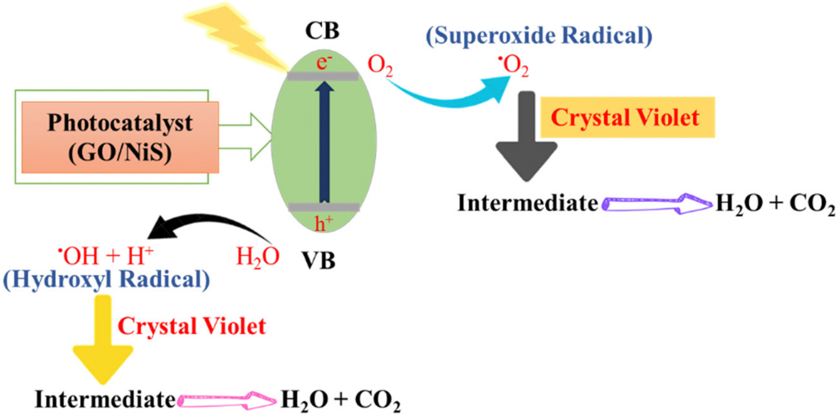
CB
e⁻
O₂
(Superoxide Radical)
·O₂
Crystal Violet
Intermediate
H₂O + CO₂
Photocatalyst (GO/NiS)
h⁺
·OH + H⁺
H₂O
VB
(Hydroxyl Radical)
Crystal Violet
Intermediate
H₂O + CO₂

Fig. 18 Photocatalytic degradation through a free radical mechanism.

break down CR dye molecules into safer components. CR dye degradation is caused by the combined activities of *OH radicals generated from CoS in the conduction band and hydrogen peroxide conversion. Radicals attack dye molecules, modifying their structure and cleaving molecular bonds, disintegrating them into non-toxic by-products. A schematic representation of the mechanism of degradation of CR in the presence of the sulfide–rGO nanocomposite is given in Fig. 20.

5.5. Photocatalysis of indigo carmine dye using NiS_2/NP

NiS_2/NP, and NiS_2/NP (1 : 10, 2 : 10, and 4 : 10) uptake were tested under identical conditions (pH 11, 20 mg L^{-1} indigo carmine, 0.2 g L^{-1} photo catalyst). The NiS_2/NP catalyst's activity increased, removing over 98% of the IC (indigo carmine) dye (20 mg L^{-1}) within 180 min of visible light exposure.[149] The reaction of conversion of indigo carmine in the presence of O_2 into isatin and then the conversion of isatin in the presence of O_2 into CO_2 and H_2O is given in Fig. 21.

5.6. Photocatalysis of crystal violet (CV), Congo red (CR) and methylene red (MR) using CoS

CoS catalyzes the reduction of dyes CV, CR and MR, which exhibit colors like purple, yellow and red. After reduction, their solutions turn colorless. Reduction experiments were conducted at room temperature with the same dye concentration, $NaBH_4$, and catalyst dosage. After reduction, their solutions turned colorless. In the absence of a catalyst, no change in absorbance was observed for hours, indicating the catalyst's crucial role in reducing organic compounds.[164] Fig. 22 presents degradation mechanism of crystal violet, methylene red and crystal red.

5.7. Science of color: an in-depth look at the features of important dyes

There are a number of significant dyes that relate to different classes of chemicals having different λ_{max} values and applications. For example, Poly R-478 is a member of the polycyclic class of dyes, showing a λ_{max} (nm) value of 520,

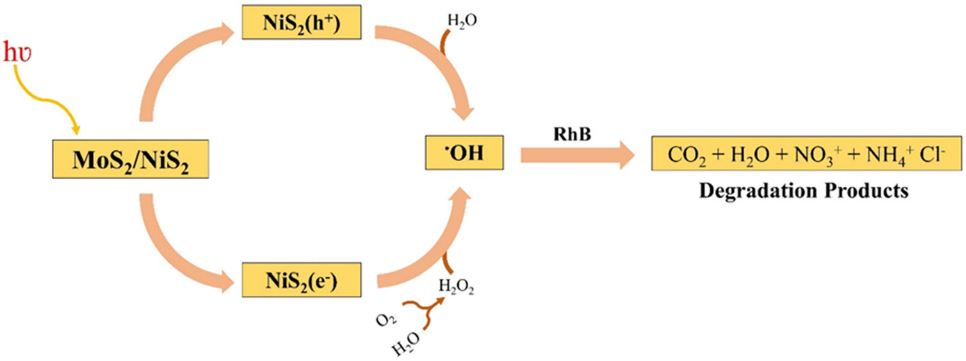

Fig. 19 Degradation of rhodamine B dye by NiS.

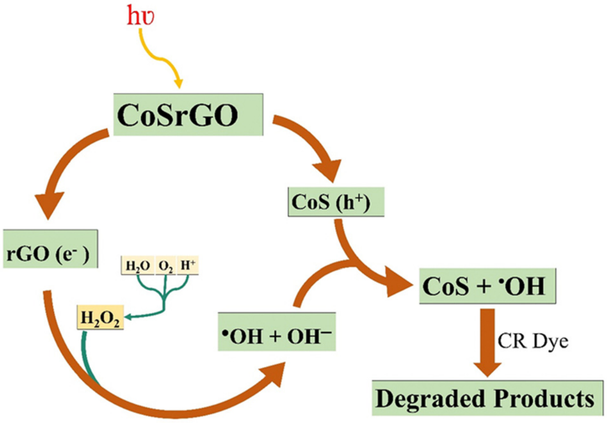

Fig. 20 CR dye degradation using CoS-rGO.

and it is used in dye-sensitized solar cells. Table 4 presents the characteristic features of some important dyes while Fig. 23 illustrates the chemical structures.

6. Dye degradation: a visual analysis of the process and results

Dye degradation is the breakdown of colored compounds in dyes, which can occur through a variety of chemical, physical, and biological processes. In a visual analysis of the process and results of dye degradation, key characteristics can be observed. Ravikumar *et al.* (2023) performed degradation of Reactive red 120 dye under a UV irradiation source. After 120 min, 93% degradation of dye was observed.[118] Table 5 represents the visual analysis of photocatalysis.

7. Advantages and disadvantages of recent advancements in electric field-assisted photocatalytic dry reforming of metals

The electric field-assisted photocatalytic dry reforming of metals is a new technology with the potential to convert carbon dioxide (CO_2) and methane (CH_4) into useful syngas (a combination of hydrogen and carbon monoxide). Although this new technique has some benefits, it also has multiple challenges that must be solved before it can be used successfully.

7.1. Advantages

Enhanced reaction kinetics. During photocatalytic dry reforming, the use of an electric field can accelerate charge separation, improve electron mobility, and stimulate catalytic activity. Because of this, reaction kinetics are enhanced, resulting in better conversion rates and a larger syngas yield.[248]

Improved selectivity. The reaction's selectivity may be influenced by an electric field aid, favoring the formation of syngas over undesirable by-products. The improved charge separation leads to a more selective and cleaner conversion process by preventing side reactions that may otherwise result in the formation of coke or carbon deposition.[249]

Lower activation energy. An electric field may reduce the activation energy needed for the reaction, allowing it to occur at lower temperatures. This minimizes the amount of energy

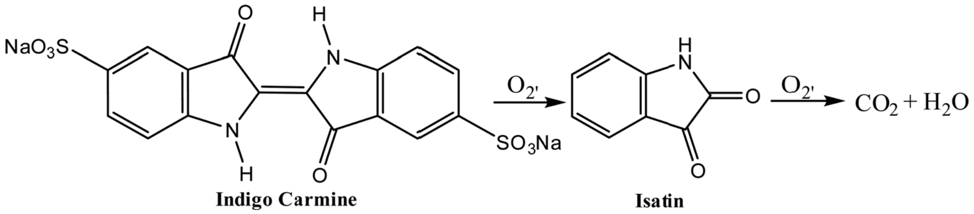

Fig. 21 Degradation of indigo carmine dye *via* NiS_2/NP photocatalysis.

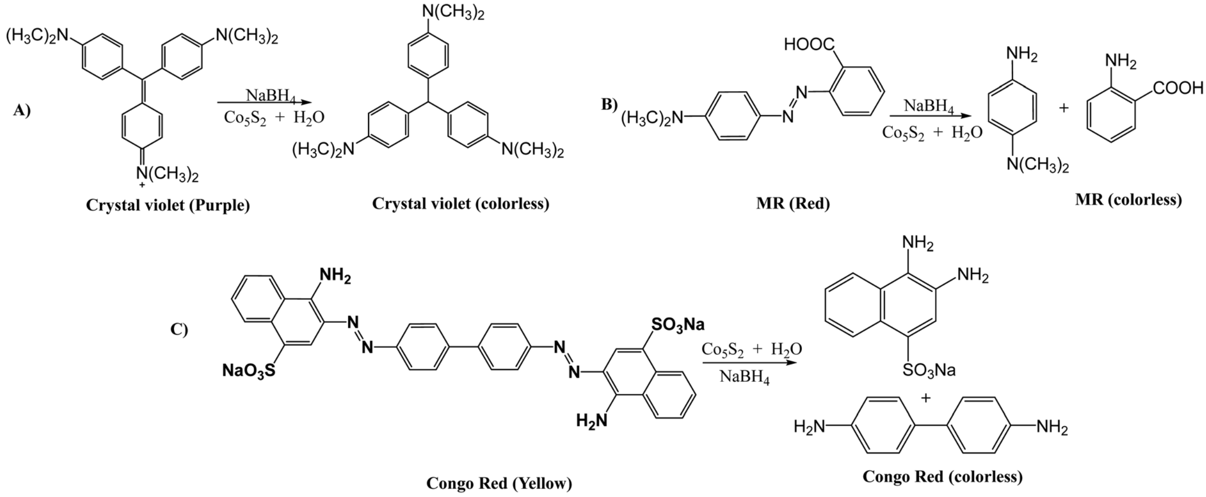

Fig. 22 Photocatalytic degradation of dyes: (A) crystal violet, (B) methylene red, and (C) Congo red.

Table 4 Comparative analysis of key characteristics for selected important dyes

Dye name	Chemical class	λ_{max} (nm)	Applications	Ref.
Poly R-478	Polycyclic	520	Dye-sensitized solar cells	218
Remazol Brilliant Blue R	Anthraquinone	595	Textile and paper industries	219
Crystal violet	Triarylmethane	590	Microbiology, textile dyes	220
Rhodamine B	Xanthene	554	Fluorescent dyes and tracers	221
Congo red	Azo	497	Textile dyes, pH indicators	222
Indigo carmine	Indigoid	610	Food coloring, pH indicators	223
Acid orange 7	Monoazo	484	Textile dyes, food coloring	224
Sudan 1	Azo	480	Oil-soluble dye, histology	225
Reactive Black 5	Azo	595	Textile dyes	226

needed and may improve the catalyst's stability under more comfortable operating conditions.[250]

Reduced catalyst deactivation. An electric field aid may minimize catalyst deactivation caused by carbon deposition because improved charge separation lowers the possibility of carbon adhesion on the catalyst surface. This results in increased catalyst lifespan and stability.[251]

7.2. Disadvantages

Complex engineering. Complex engineering and design concerns need to be considered for implementing electric field-assisted photocatalytic devices. The incorporation of electrodes, power supplies, and reaction chambers complicates the setup and may present difficulties in scaling up the process.[252]

Energy consumption. Reaction kinetics can be improved by electric fields, but they also need energy to operate. Especially, in the context of the process's overall energy efficiency, the energy used to generate and sustain the electric field should be carefully evaluated.[253]

Electrode fouling. Electric fields may cause electrode fouling or deterioration over time owing to electrode material corrosion or reaction byproduct buildup. This may have an effect on the stability and efficiency of electric field generation.[254]

Cost considerations. The use of an electric field aid can result in extra expenditures for equipment, power sources, and upkeep. To determine the economic viability of the technology, a complete cost-benefit analysis is required.[255]

8. Density functional theory (DFT) studies on metal sulfide nanoparticles for dye degradation

The adoption of density functional theory (DFT) has become increasingly prevalent as a powerful computational instrument in the investigation of the electronic configuration, optical characteristics, and adsorption tendencies of nanomaterials. Metal sulfide nanoparticles have been extensively studied due to their unique properties and potential applications in various fields.[256] One of the key aspects of their characterization involves understanding the energetics of dye adsorption, reaction pathways, and reaction mechanisms. In this regard, density functional theory calculations have emerged as a powerful tool for gaining insights into these fundamental aspects. By employing DFT, researchers are able to computationally investigate the interactions between metal sulphide nanoparticles and dyes, thereby providing valuable information regarding the thermodynamics and kinetics of the adsorption process.[257] Furthermore, DFT calculations enable the exploration of different reaction pathways and mechanisms, shedding

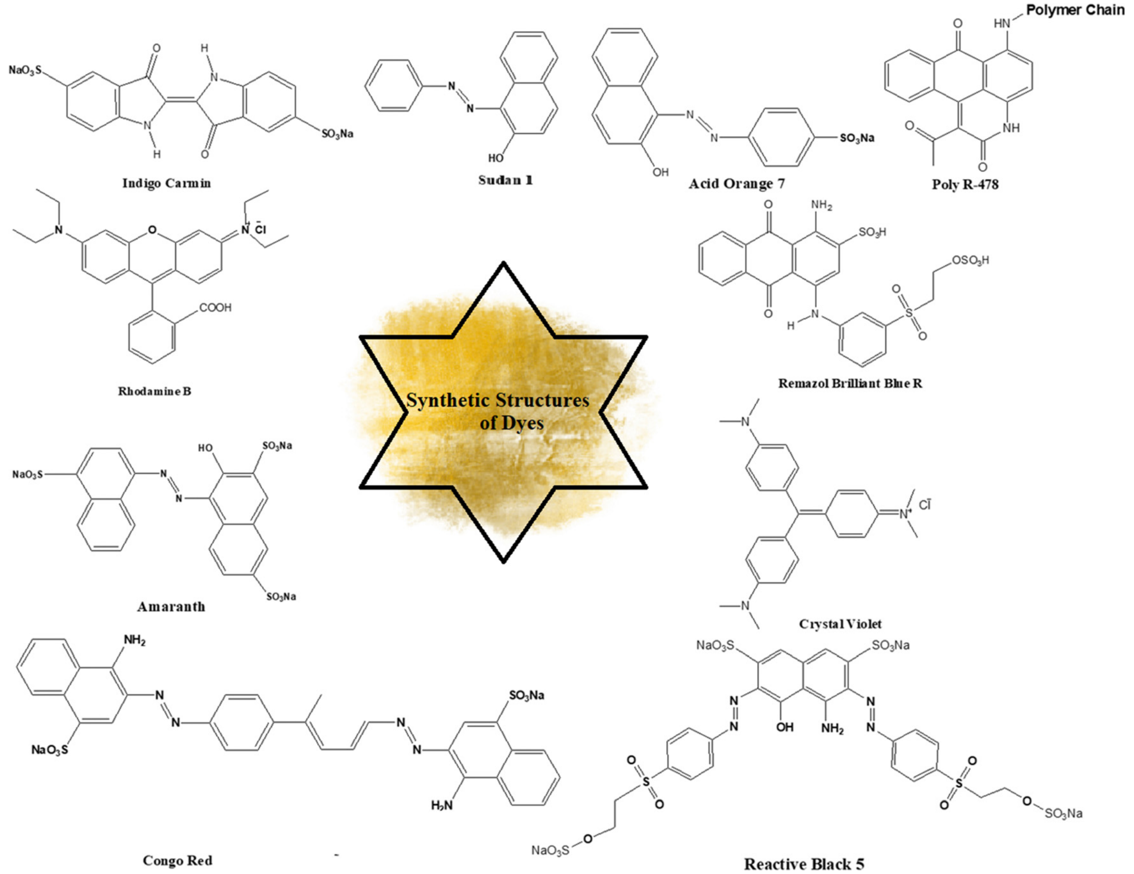

Fig. 23 Comparative analysis of chemical structures for key synthetic dyes.

light on the underlying chemical transformations occurring on the nanoparticle surface. Consequently, the utilization of DFT in the study of metal sulphide nanoparticles has significantly contributed to our understanding of their behavior and has paved the way for the development of novel applications in fields such as catalysis, energy storage, and sensing.[258]

8.1. Adsorption of dye molecules on metal sulfide nanoparticles

The use of DFT has provided us with the ability to make predictions about the adsorption behavior of dye molecules on metal sulphide nanoparticles. The interaction strength, preferred adsorption sites, and charge transfer pathways may all be clarified *via* the use of these simulations. The adsorption energies that are predicted using DFT give vital information that is necessary for understanding the stability of the dye-nanoparticle complexes and the possibility for effective dye degradation.[259]

8.2. Reaction pathways and mechanisms

The incorporation of density functional theory (DFT) studies provides a pathway for the investigation and examination of the complex reaction pathways and underlying mechanisms implicated in the process of dye degradation on metal sulphide nanoparticles. Through careful examination and investigation of the transition states and reaction intermediates, valuable insights can be obtained regarding the pivotal steps that dictate the overall rate of the reaction and the possible pathways that the reaction may follow.[260] The discovery of these aforementioned insights holds paramount importance in the realm of designing and optimizing metal sulphide nanoparticles with the ultimate objective of achieving optimal efficacy in the degradation of dyes.[261]

8.3. Role of metal sulfide composition and morphology

DFT calculations may help us understand how the composition and form of metal sulphide nanoparticles impact the catalytic activity of these particles in the process of dye degradation. We can detect patterns and connections between the electronic structure and catalytic performance by conducting in-depth research on a variety of metal sulphide morphologies and compositions.[262]

9. Optimization strategies for the degradation of metal sulfides

The optimization strategies for degrading metal sulfides can be categorized into two primary classes. The first class involves a conventional kinetic approach, while the second utilizes the more advanced response surface methodology (RSM).

Table 5 A visual guide for understanding dye degradation characteristics and features

Sr. no.	Dye used	Reaction conditions			Degradation (%)	Ref.
		Dose (mg)	pH	Time (min)		
01.	Indigo carmine	—	—	240	78	1
02.	Reactive red 120	50	5	120	93	118
03.	Methyl orange	—	—	90	87	227
04.	Methylene blue	0.211	—	180	62	120
05.	Methylene blue	100	—	60	100	121
06	Eosin B	0.03	—	160	95	122
07.	Methyl blue	—	—	10	99.97	123
08.	Rhodamine B	—	—	180	92	27
09.	Methylene blue	20	—	120	100	124
10.	Methylene blue	0.2	—	45	100	125
11.	Rhodamine B	0.1	—	90	98.8	126
12.	Malachite green oxalate	1.5	9	120	90.7	127
13.	Methyl orange	25	—	150	97.1	128
14.	Reactive red 141	50		180	98	129
15.	Orange red	20	10	180	93	130
16.	Methylene blue	0.5–2	—	30	98.26	131
17.	Methyl violet	—	—	90	91.8	131
18.	Rhodamine B	—		120	64.1	132
19.	Methylene blue	10	—	30	100	78
20.	Cationic methylene blue	100	—	270	99.04	133
21.	Rhodamine B	10	—	240	63	134
22.	Methyl orange	10	—	240	78	134
23.	Rhodamine B	—	—	—	93	135
24.	Rhodamine B	10	—	120	88	136
25.	Methylene blue	100	—	90	99.0 ± 0.4	137
26.	Methylene blue	—	—	180	90	138
27.	Indigo carmine	100	—	240	85.30	139
28.	Rhodamine B	238.43	—	90	90.2	140
29.	Reactive red 141	50	—	240	73	141
30.	Rhodamine B	—	—	15	85	142
31.	Rhodamine B	50	—	40	90	143
32.	Methylene blue	10	—	25	7	144
33.	Rhodamine B	50	—	40	100	145
34.	Rhodamine B	5	—	120	82	146
35.	Methylene blue	—	—	60	71	147
36.	Rhodamine B Methylene blue	—	—	180	71 59	148
37.	Indigo carmine	1000	—	180	98	149
38.	Methylene blue Rhodamine-B	—	—	180	91 92	150
39.	Indigo carmine	100	7	240	51	1
40.	Methylene blue	3	—	140	56.3	151
41.	Methylene blue	5	—	70	89	14
42.	Crystal violet	20	—	60–80	91	152
43.	Amido black	10	2–10	300–420	98	153
44.	Methylene blue	5	—	20	56	154
45.	Methyl orange	10	2	90	7.9	155
46.	Rhodamine-B	—	—	120	87	156
47.	Eosin yellow	—	10	540	—	157
48.	Methylene blue	—	3–7	30–100	87	158
49.	Methylene blue	—	—	10	99	159
50.	Methyl blue	50	8.5	300	93.6	17
51.	Cr(VI)	1000	2–10	200	57.05	160
52.	Eosin yellow	50	10	360	100	161
53.	Rhodamine-B	100	—	30	—	162
54.	Methylene blue	100	—	180	94	163
55.	Crystal violet	—	—	120	76	164
56.	Congo red	1000	3–11	120	57.89	13
57.	Methyl orange	100	—	50	98	165
58.	Methylene blue	200	—	80	5	166
59.	Rhodamine-B	1000	—	75	96	167
60.	Congo red	5	7	—	90	168
61.	Methylene blue	5	—	90	88	169
62.	Methylene blue	20	12	120	76–78	228
63.	Methylene blue	0.01	—	240	81	229
64.	Methylene blue	10	—	40	98.25	170
65.	Methyl red	—	10	50	95.01	171
66.	Methylene blue	10	—	—	54.4	172
67.	Methylene blue	—	4–7	—	—	173

Table 5 (*continued*)

		Reaction conditions				
Sr. no.	Dye used	Dose (mg)	pH	Time (min)	Degradation (%)	Ref.
68.	Azure B	100	8	240	90	174
69.	Congo red	5	12	10	50–60	175
70.	Methylene blue	114	—	220	91.8	176
71.	Methylene blue	60	—	105	9	230
72.	Brilliant green	500	—	30	—	178
73.	Crystal violet	—	—	40	98.5	231
74.	Indigo carmine	—	—	—	88	1
75.	Rhodamine B	—	—	180	92	27
76.	Methylene blue	—	—	220	91.8	176
77.	Methyl green	10	2	120	91	232
78.	Congo red	—	—	40	97.03	13
79.	Methylene blue	20	6.8	10	99.8	17
80.	Methylene blue	—	—	50	96	14
81.	Rhodamine B	—	—	150	85	28
82.	Methylene blue	250	—	10	99.97	233
83.	Congo red	20	—	60	94.9	234
84.	Indigo carmine	200	—	—	88	1
85.	Brilliant green	10	7	60	95%	235
86.	Crystalline violet	5.0	11	90	98.5	236
87.	A-2bng	40	7.5	120	98.17	237
88.	Methylene blue	5	—	220	91.8	176
89.	Methylene blue	—	—	180	75.02	238
90.	MO-Rhb	—	4.45–10.38	60	98 96	239
91.	Rhodamine B	—	—	25	96	240
92.	Rhodamine B	0.00125	9	116	87.53	241
93.	4,5-Dibromofluorescein	—	—	<30	97	242
94.	Brilliant green	—	—	90	95	243
95.	Azo dye	—	—	—	88	244
96.	Rhodamine B	—	2.9	150	~89	245
97.	Methylene blue	—	—	240	70	246
98.	Rhodamine B	—	—	—	—	247
99.	Congo red	—	—	100	100	206
100.	Methyl orange	—	2–9	90	93	207

9.1. Conventional optimization approach

Most photocatalytic reactions are optimized using the traditional kinetic approach, in which the influence of reaction parameters (including photocatalyst concentration, dye molecule concentration, irradiation time, and pH) on the response (percentage degradation; %*D*) is investigated by varying one reaction parameter and measuring its influence on %*D* while keeping all other reaction parameters constant.[263–267] This optimization method assumes that all reaction parameters are independent of one another and that there is no connection between these reaction parameters. Danish *et al.* (2021) employed the conventional kinetic approach for the degradation of MB dye. The MB concentration ranged from 15 to 65 ppm, with the highest degradation efficiency, 93.53%, occurring at 45 ppm. Beyond this point, the degradation rate declined quickly. This is expected since, initially, NCs' active sites can absorb extra MB, leading to rapid degradation until the optimal 45 ppm level is attained.[32]

Ebrahimi *et al.* (2022) examined the factors influencing the photocatalytic degradation of MC-LR. Key aspects, such as pH, contact duration, and catalyst quantity, were considered in the conventional method. The breakdown of MC-LR by BiVO$_4$ was predominantly influenced by pH, exposure time, and catalyst dosage, as indicated by high mean square and *F*-value metrics. The most crucial factor was the catalyst amount, with mean square and *F*-value readings of 608.58 and 181.98, respectively. pH and contact time were of lesser importance. The study aimed to investigate MC-LR removal at varying pH levels, ranging from 5 to 9, and found that pH had a negative impact on MC-LR elimination.[268] The novel photocatalyst tBiPO$_4$/Bi$_2$S$_3$-HKUST-1-MOF was synthesized by Mosleh *et al.* (2016) and photocatalysis optimization of parameters like exposure duration, pH, catalyst quantity, spin rate, liquid flow, air supply, toluidine blue and auramine-O dye concentrations was performed. Ideal values are: 65 min, 6, 0.25 g L^{-1}, 1300 rpm, 0.40 L min^{-1}, 35 L min^{-1}, 25, and 25 mg L^{-1}, respectively. Under these conditions, TB and AO degradation reached 99.37% and 98.44%, with a desirability of 1.0.[269] Fig. 24 illustrates the impact of reaction parameters on %*D* values.

9.2. Response surface methodology (RSM) optimization approach

Response surface methodology (RSM) is a tool that is used in photocatalysis to optimize and model the relationship between experimental variables and photocatalytic performance. It involves setting up a series of experiments with different

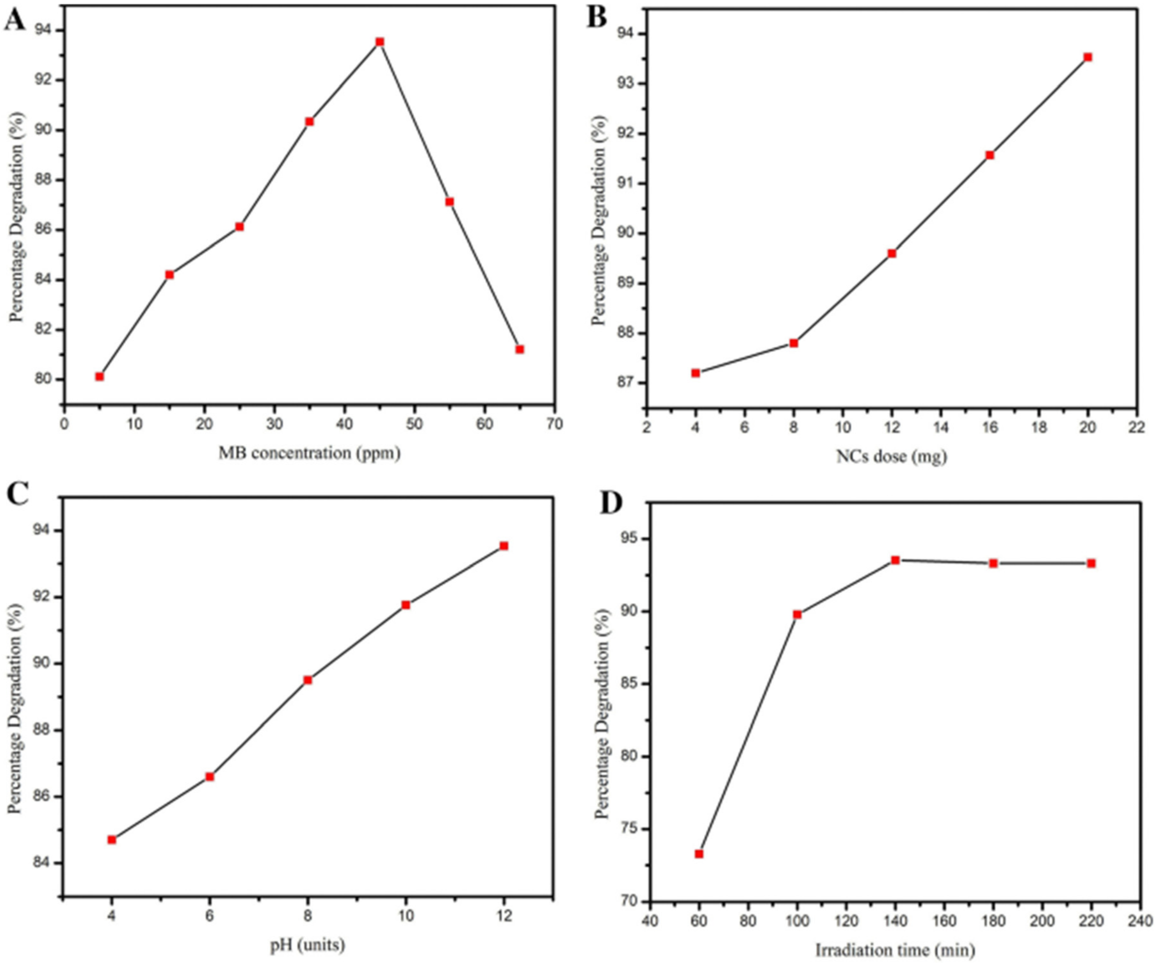

Fig. 24 Impact of reaction parameters (A) concentration of dye, (B) pH values, (C) dose of catalyst, and (D) irradiation time on %*D* values. Reproduced with permission[32] Copyright 2021 Springer Nature.

combinations of independent variables to find the best conditions for getting the desired result.[270] RSM is particularly useful for studying complex reaction mechanisms and identifying the key factors that influence photocatalytic performance (Fig. 25).[271] RSM helps researchers to find out the best conditions for maximizing the effectiveness of photocatalysis by giving them a mathematical model of the relationship between the input variables and the output response.[272] Furthermore, RSM can also be used to optimize the synthesis and preparation of photocatalysts as well as the operating parameters of the photocatalytic process.[271] Overall, RSM is a valuable tool for designing and optimizing photocatalytic processes, and its application is expected to continue to grow in the field of photocatalysis.

9.2.1. Evaluation of independent variables and selection of desired responses. The first and the most important stage in the procedure for employing RSM in the dye removal process is to recognize the independent variables that influence the procedure.[273] It is crucial to select responses that have a significant impact on the pigment removal procedure and are independent of one another. Moreover, the ranges of these selected factors must be determined based on the results of previous evaluations.[274] Several environmental parameters, such as reaction time, pH, and initial dye concentration, have a significant impact on the physicochemical removal of dyes.[275] These parameters may vary based on the specified coloring agent removal method.[275]

9.2.2. Choosing the experimental design strategy. The choice of a suitable design strategy has a significant impact on the creation of a response surface and the accuracy of the predicted model. For physicochemical removal of dyes, the main design strategies are full factorial design (FFD),[276] central composite design (CCD),[277–279] Box–Behnken design (BBD),[280–282] and Doehlert design (DD) (Fig. 26).[283] There are a number of computer programs that facilitate the use of these procedures. Minitab,[284] Design Expert,[285] Statistica and MATLAB are popular software applications for employing DOE for physicochemical removal of pigments.[286]

Full factorial design. The full factorial design method is a standard experimental design with 2–3 input variable levels.[287] The two-level FFD generates 2K designs, accounting for low and high values for each factor.[288] The three-level FFD creates 3K patterns with factors having low, middle, or high values.[289] For fewer than five variables, the 3-k FFD is more useful.[290,291]

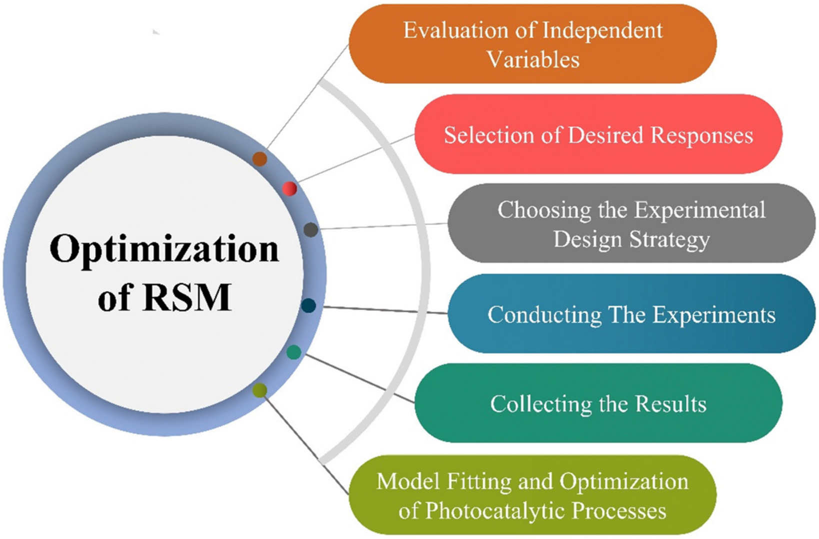
Optimization of RSM
Evaluation of Independent Variables
Selection of Desired Responses
Choosing the Experimental Design Strategy
Conducting The Experiments
Collecting the Results
Model Fitting and Optimization of Photocatalytic Processes

Fig. 25 The optimization of physicochemical processes using RSM consists of six sequential steps.

Full Factorial Design
Design of Central Composite
Choosing the Experimental Design Strategy
Doehlert Design
Box–Behnken Design

Fig. 26 Choosing the experimental design strategy for degradation of dye.

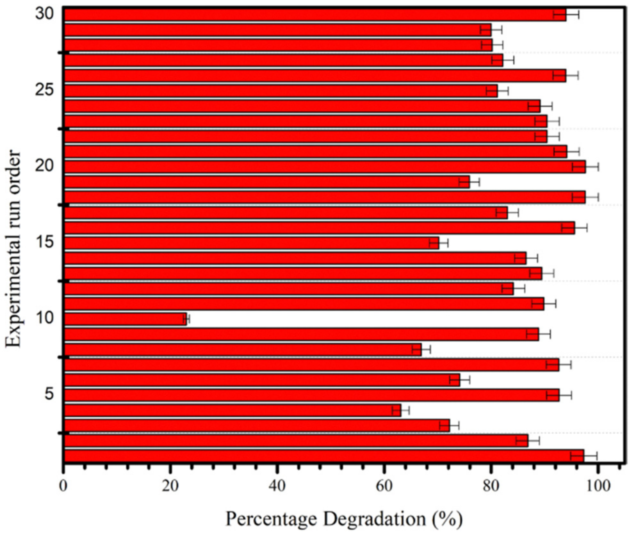

Fig. 27 CCD-based %*D* values obtained from thirty experimental runs conducted to study the photocatalytic degradation reaction of MB. Reproduced with permission[32] Copyright 2021 Springer Nature.

Design of central composites. CCD is the most commonly used design technique in environmental systems for creating second-order reaction surface models.[292] The CCD gives the same information as the three-level FFD but with far fewer trial tests.[293] Furthermore, CCD predicts the linear and quadratic interaction impacts of variables affecting the chosen procedure.[294] Fig. 27 represents the CCD-based %*D* values of MB dye obtained from thirty experiments. Roya Tangsiri *et al.* (2020) synthesized CdS nanoparticles and utilized them to photodegrade ranitidine. Design studies utilizing a central composite design with response surface methodology investigated the simultaneous impacts of the influencing factors. The best RD (ranitidine degradation) was achieved at pH 6.2, a catalyst dosage of 0.6 g L^{-1}, a ranitidine concentration of 3.4 mg L^{-1}, and an irradiation period of 97.5 min. The quadratic polynomial model's strong correlation coefficient (R^2 = 0.9739) demonstrated that RSM data matched experimental data.[295] Arash *et al.* (2016) prepared manganese-impregnated zinc sulfide nanoparticles on activated carbon (ZnS: Mn-NPs-AC) and evaluated to remove malachite green and methylene blue in binary combination. Their removal efficiency was evaluated using the central composite design. Results from multiple regression analyses and 3-D response surface and contour plots indicated that a pH of 7.0, 3 min sonication time, 0.025 g Mn: ZnS-NPs-AC, and 15 mg L^{-1} MB and MG result in 99.87% and 98.56% removal efficiencies, respectively.[296]

Box–Behnken design. This concept was created by Box and Behnken[297] and is a useful tool for conducting experiments as it provides three levels (−1, 0, +1) for each variable, and $N = 2k(k_1) + C_0$ represents the total number of experiments required, where k is the number of variables and C_0 is the number of central points.[280] This design is depicted as a cube, with all points located on a sphere with a radius of 2, and does not include any points at the vertices in the region formed by the upper and lower limits of each variable. The gold nanoparticle-loaded mesoporous TiO_2 photocatalysts for ibuprofen (IBP) mineralization in an aqueous heterogeneous suspension were synthesized by Alaa *et al.* (2022). The photocatalytic process was optimized using a Box–Behnken design using response surface methodology (RSM) with three variables and three stages. An optimal IBP mineralization efficiency of 98.50% was achieved with 366 nm wavelength irradiation, 29.46 mg L^{-1} IBP concentration, and 0.5 wt% metal concentration.[297] Hassan *et al.* (2023) studied response surface methodology and the Box–Behnken model to determine the synergistic effects of three independent experimental parameters (hormone concentration, solution pH, and photocatalyst dosage) on silica-supported g-C_3N_4/WO_3 nanocomposites with enhanced estrone hormone degradation. These testing conditions resulted in 100% and 96% hormone photodegradation after 3 h of UV and visible light irradiation.[282]

Doehlert design. Doehlert invented the symmetrical shell shape to support different levels of variation in variables, like major and minor levels. It is useful when studying variables with limitations, such as cost or time constraints.[298] The Doehlert design has a regular distribution between each degree of each component. To determine the number of trials needed, the equation $N = k_2 + k + C_0$ is used. For two factors, the design is a regular hexagon with six hexagonal points surrounding a center point.[299] For three variables, a cuboctahedron is used, which has high productivity and needs fewer trial points.[300]

9.2.3. Conducting the experiments and collecting the results. After choosing the right design strategy and setting up the design level values, computer software can be used to set up a series of experiments in a certain order.[301] After the experiments are done, the results are analyzed using the design strategy, which leads to a mathematical model. To prove that the whole process works, this mathematical model needs to be changed to fit the experimental data.[302]

9.2.4. Model fitting and optimization of photocatalytic processes. In conventional methods for determining this relationship, experiments are conducted by systematically modifying the studied parameter while keeping all other parameters constant.[303] In addition, this extensive procedure cannot identify the combined effect of the effective parameters. Thus, empirical evidence regarding the relationship between factors and response must be gathered. Moztahida and Lee *et al.* (2020) optimized PGP-0.5 hydrogels' photocatalytic MB elimination. pH, temperature, and MB concentration were key factors. A 3K Box–Behnken model improved critical parameters for high efficiency in water-rich liquids. Measurements were represented by numbers (1, 0, or 1) indicating low, middle, or high values, respectively.[31] Fathinia *et al.* (2010) optimized the photocatalytic decolorization of two dyes (AB92 and BB3) using a central composite design of response surface methodology. Four variables (starting dye content, UV light strength, flow rate, and reaction time) were tested, and a total of 31 trials were conducted for each dye. Minitab 15 was used to analyze the experimental data.[304] Sahoo and Gupta *et al.* (2012) utilized a single factor study to identify significant factors affecting the photocatalytic degradation of MB, selecting the catalyst dosage, starting pigment content, and pH as variables. Using RSM, these factors were optimized as independent variables with COD and color elimination as response variables and evaluated through 15 sets of Box–Behnken trials.[305]

9.3. Distinctive perspectives on RSM optimization

Integration of machine learning. The combination of response surface methodology with machine learning algorithms has the potential to improve the precision of predicting optimal conditions. This integration facilitates the expeditious and precise determination of synthesis parameters.[306]

Consideration of environmental impact assessment. In addition to the catalytic efficiency, it is imperative for RSM optimization to also take into account the environmental implications associated with the synthesis methods employed. The implementation of strategies aimed at reducing waste, energy consumption, and the generation of hazardous by-products has the potential to foster the development of more sustainable processes for the synthesis of metal sulfide nanoparticles.[307]

9.4. Modification strategies for optimizing response surface methodology of metal sulfide nanoparticles in dye degradation

The utilization of response surface methodology (RSM) in the optimization of the synthesis process for metal sulfide nanoparticles has been demonstrated to be highly advantageous in attaining improved efficiency in dye degradation. In order to enhance the efficacy of this methodology, it is crucial to contemplate a multitude of modification strategies that have the potential to optimize photocatalytic performance and improve environmental impacts.[32]

9.4.1. Modification strategies for RSM optimization. The subsequent section of this paper shall undertake a comprehensive exploration of diverse modification strategies that can be effectively implemented to enhance the efficiency and efficacy of the response surface methodology in the synthesis of metal sulfide nanoparticles.

Amorphous single atoms and diatomic research. The incredible catalytic capabilities of amorphous single atom and diatomic structures have drawn attention lately. The integration of these configurations into metal sulfide nanoparticles has been shown to enhance the efficiency of dye degradation. This is achieved by facilitating a greater number of active sites and improving the surface area available for catalytic reactions.[308] The subsequent section of this paper shall undertake a comprehensive exploration of diverse modification strategies that can be effectively implemented to enhance the efficiency and effectiveness of the response surface methodology in the synthesis of metal sulfide nanoparticles.

van der Waals heterojunctions. The concept of van der Waals heterojunctions revolves around the deliberate manipulation and organization of distinct materials possessing complementary characteristics, thereby leading to the emergence of synergistic phenomena.[309] The integration of heterojunctions within metal sulfide nanoparticles has been shown to enhance their charge separation capabilities and expand their light absorption range. Consequently, this integration has the potential to significantly enhance the photocatalytic performance of these nanoparticles in the context of dye degradation.[310]

Microenvironment regulation. The optimization of photocatalytic activity in metal sulfide nanoparticles is heavily influenced by the meticulous adjustment of their microenvironment. The manipulation of various parameters, such as pH, temperature, and gas atmosphere, during the synthesis process has been found to have a significant impact on the surface states and band positions of catalysts. Consequently, these alterations in surface properties and electronic band structures have been observed to induce changes in the catalytic behavior of the materials under investigation.[311]

Amorphous 2D layered material coupling. The combination of amorphous two-dimensional (2D) layered materials with metal sulfide nanoparticles has the potential to enhance photocatalytic reactions. The utilization of composite structures in various applications has drawn significant attention due to their ability to offer a high surface area, thereby facilitating efficient charge transport. In the context of dye degradation, the incorporation of composite structures has been found to yield notable improvements.[312]

9.5. Advantages of the RSM

1. Through RSM, the catalytic effectiveness and specificity may be increased by adjusting the nanoparticles' size, shape, and surface characteristics.[313]
2. It is possible to synthesize nanoparticles with unique and advantageous characteristics using sustainable and biologically friendly reagents and circumstances.[314]
3. Better dye degradation performance may be achieved *via* the production of nanoparticles with multifunctional properties like magnetic responsiveness or tailored distribution.[315]
4. More precise control over synthesis may be achieved by using sophisticated real-time monitoring tools, which guarantee that the required features are attained.[316]

9.6. Addressing stability challenges in optimizing response surface methodology for metal sulfide nanoparticle synthesis for dye degradation

The utilization of response surface methodology (RSM) has garnered significant attention as a potent instrument for optimizing a diverse range of chemical processes. One such application involves the synthesis of metal sulfide nanoparticles, specifically for the purpose of dye degradation.[275] The utilization of response surface methodology provides a significant explanation of the connections between various factors and the desired result. However, it is crucial to set priorities for the establishment of stability within the optimization process.

Challenges in stability. The synthesis of metal sulfide nanoparticles necessitates the optimization of various parameters simultaneously, a practice that may potentially introduce instability into the optimization procedure. The reproducibility of the optimized synthesis may be prevented by the presence of inconsistent results, which can arise from fluctuations in environmental conditions, reagent concentrations, and reaction kinetics.[317] The presence of instability within the research not only undermines its credibility but also imposes constraints on its potential for practical implementation in real-world contexts.

Leveraging control variables. In order to tackle the issues of stability, scientists might deliberately choose and manage factors that have a substantial influence on the synthesis process. Through the utilization of methodologies such as design of experiments,[318] the identification of the most influential variables can be achieved, thereby enabling the refinement of the optimization process to yield outcomes that are both consistent and reproducible. Furthermore, the incorporation of process control mechanisms that possess the capability to autonomously adapt variables in accordance with alterations in the surrounding environment can effectively alleviate the adverse effects caused by fluctuations.[319]

Incorporating *in situ* monitoring. Monitoring the real-time synthesis process can yield crucial information regarding its stability. By employing techniques such as electron microscopy, chromatography, and spectroscopy, scientists can track alterations in nanoparticles and identify deviations from the optimal pathway. In addition to facilitating the detection of stability issues, the practice of *in situ* monitoring enables swift implementation of corrective measures[320]

Validation and sensitivity analysis. In order to ascertain the stability of the optimized synthesis, it is imperative to undertake a series of repeated experiments under diverse conditions. The assessment of the optimization process's robustness and its ability to withstand minor fluctuations is facilitated by this approach. The utilization of sensitivity analysis facilitates the identification of variables that exhibit heightened sensitivity towards stability issues, thereby empowering researchers to focus their efforts on the prioritization of control measures.[321]

10. Challenges and future prospects

This paper discusses the challenges and future trends in the synthesis of metal sulfide nanoparticles and their application in the degradation of dyes using conventional and response surface methodology (RSM) approaches. It also discusses the limitations of current methods, identifies research gaps, and proposes potential strategies to overcome existing challenges and enhance the performance of metal sulfide nanoparticles in dye degradation.

Challenges

1. Developing synthetic methods that can precisely control the size, shape, and crystal structure of MSNPs to enhance their performance in dye degradation.

2. Ensuring that the synthetic methods are both reproducible and scalable to enable industrial-scale synthesis of metal sulfide nanoparticles.

3. Developing environmentally friendly and cost-effective synthetic approaches to reduce the environmental impact and improve the economic viability of metal sulfide nanoparticles.

4. Improving the efficiency, stability, and reusability of metal sulfide nanoparticles in dye degradation applications to ensure their long-term effectiveness and sustainability.

5. Enhancing the selectivity and specificity of MNPs for different types of dyes.

6. Assessing and mitigating the potential toxicity and environmental impact of metal sulfide nanoparticles.

7. Addressing the limitations of conventional approaches in optimizing metal sulfide-based dye degradation systems.

8. Overcoming the challenges in implementing RSM for metal sulfide nanoparticle-based dye degradation.

Future prospects

1. Developing and investigating novel, eco-friendly, and cost-effective metal sulfide nanoparticles that allow precise control over their properties.

2. New strategies should be adopted to enhance the photocatalytic, adsorption, and redox capabilities.

3. Exploring the integration of conventional and RSM approaches with other optimization techniques, such as machine learning and artificial intelligence.

4. Encouraging collaborations among material scientists, environmental engineers, and industry experts to accelerate the development and implementation of innovative metal sulfide nanoparticles.

The recently suggested strategies for modification exhibit considerable potential for advancements in the area of photocatalysis. The utilization of doors in the context of innovative designs and tailored photocatalysts has been observed to provide opportunities for optimization in specific dye degradation applications. This comprehensive overview aims to provide researchers with strategies that can effectively guide their efforts. By seeking the information presented herein, researchers embarking on new studies can gain valuable insights and guidance to inform their research attempts.

11. Conclusions

In conclusion, the synthesis of metal sulfide nanoparticles and their use in the degradation of dyes using both traditional and response surface methodology approaches hold significant potential to help in solving problems caused by synthetic dyes that cause environmental remediation. Due to the high surface area, tunable bandgap, and strong redox capabilities, metal sulfide nanoparticles have become promising materials for the efficient degradation of environmental polluted dyes. This review provides insights into a comprehensive understanding of the diverse synthetic approaches. By tailoring the properties of these nanoparticles, researchers can optimize their performance in dye degradation applications. Moreover, the discussion of the different mechanisms involved in dye degradation, such as photocatalytic, adsorption, and redox processes, has shed light on the different factors that affect the efficiency of MSNPs. The conventional approaches have demonstrated promising results in the degradation of dyes using nanoparticles. As a powerful statistical tool, RSM has been shown to be an upright mode to improve the performance of nanomaterials in dye degradation systems to optimize the process parameters. By studying both the traditional and RSM approaches together, researchers can be more efficient and can gain a better understanding of the synthesis and photocatalytic processes. This study sheds light on the use of MSNPs in the real world for breaking down the effluents. The problems like stability, reusability, and selectivity of the NPs need further research and development in this area. Researchers can find ways to improve the performance of metal sulfide nanoparticles in environmental applications by identifying future research opportunities.

Conflicts of interest

There are no conflicts to declare.

Acknowledgements

The authors extend their appreciation to the research center for Advanced Materials Science (RCAMS)" at King Khalid University, Saudi Arabia, for funding this work under the grant number RCAMS/KKU/016-22.

References

1 A. M. Huerta-Flores, L. M. Torres-Martínez, E. Moctezuma, A. P. Singh and B. Wickman, *J. Mater. Sci.: Mater. Electron.*, 2018, **29**, 11613–11626.
2 H. Zhang, Z. Wang, J. Zhang and K. Dai, *Chin. J. Catal.*, 2023, **49**, 42–67.
3 A. Ghorbani-Choghamarani and Z. Taherinia, *Mol. Catal.*, 2023, **535**, 112829.
4 H.-Q. Chen, J.-G. Hao, Y. Wei, W.-Y. Huang, J.-L. Zhang, T. Deng, K. Yang and K.-Q. Lu, *Catalysts*, 2023, **13**, 544.
5 Z. Li, Y. Wang, K. Chen, J. Tang, L. Liu and W. Huang, *J. Alloys Compd.*, 2023, **943**, 169170.
6 J. Wang, J. Yang, H. Yang, H. Huang, X. Yang and L. Wei, *Opt. Mater.*, 2023, **135**, 113303.
7 S.-l Zhou, L.-g Gong, X.-y Zhao, Q.-l Liang, W.-j Zhang, L.-y Wang, K. Yu and B.-b Zhou, *Chem. Phys. Lett.*, 2020, **759**, 138034.
8 A. Singh, A. Ahmed, A. Sharma, C. Sharma, S. Paul, A. Khosla, V. Gupta and S. Arya, *Phys. B*, 2021, **616**, 413121.
9 M. Sankar, M. Jothibas, A. Muthuvel, A. Rajeshwari and S. J. Jeyakumar, *Surf. Interfaces*, 2020, **21**, 100775.

10 C. Balischewski, H. S. Choi, K. Behrens, A. Beqiraj, T. Körzdörfer, A. Geßner, A. Wedel and A. Taubert, *ChemistryOpen*, 2021, **10**, 272–295.

11 H. Peng, Y. Du, J. Yong, C. Huang, X. Zheng and J. Wen, *Chem. Eng. J.*, 2023, **452**, 139386.

12 C. Zhang, L. Fu, B. Yao, J. Zhu, W. Yang, D. Li and L. Zhou, *ACS Appl. Mater. Interfaces*, 2023, **15**, 8022–8032.

13 P. Borthakur and M. R. Das, *J. Colloid Interface Sci.*, 2018, **516**, 342–354.

14 S. Haider, S. S. Shar, I. Shakir and P. O. Agboola, *Ceram. Int.*, 2021, **47**, 34269–34277.

15 F. Chen, H. Yang, X. Wang and H. Yu, *Chin. J. Catal.*, 2017, **38**, 296–304.

16 J. Bai, W. Chen, R. Shen, Z. Jiang, P. Zhang, W. Liu and X. Li, *J. Mater. Sci. Technol.*, 2022, **112**, 85–95.

17 A. A. Khan, S. Kumari, A. Chowdhury and S. Hussain, *ACS Appl. Nano Mater.*, 2018, **1**, 3474–3485.

18 E. Horozić, Z. Ademović, J. Suljagić, A. Cipurković, E. Roša, A. Sejfić, D. Husejnagić and S. Hodžić, *Technol. Acta: Sci. Prof. J. Chem. Technol.*, 2019, **12**, 27–30.

19 W. Li, S. Li, Y. Tang, X. Yang, W. Zhang, X. Zhang, H. Chai and Y. Huang, *J. Hazard. Mater.*, 2020, **389**, 121856.

20 C. Deng, X. Ling, L. Peng, T. Wang, R. Xu, Y. Zhu, W. Zhang, P. Sun, Y. Wu and H. Hu, *Appl. Surf. Sci.*, 2023, 157065.

21 Z. Yuan, J. Zou, X. Zhao, J. Shi, C. Guo and M. Yan, *Journal of Materials Science & Technology*, 2023, **166**(10), 86–97.

22 A. A. Yaqoob, C. Guerrero–Barajas, A. Ahmad, M. N. M. Ibrahim and M. B. Alshammari, *Green Chem. Sustainable Water Purif.*, 2023, 179–202.

23 W.-K. Jo and R. J. Tayade, *Chin. J. Catal.*, 2014, **35**, 1781–1792.

24 E. Issaka, S. Yakubu, H. Sulemana, A. Kerkula and O. Nyame-do Aniagyei, *Chem. Eng. J. Adv.*, 2023, 100449.

25 V. Devra, *Fungal Cell Factories for Sustainable Nanomaterials Productions and Agricultural Applications*, Elsevier, 2023, pp. 257–288.

26 Q. Jiang, C. Ji, D. J. Riley and F. Xie, *Nanomaterials*, 2018, **9**, 1.

27 M. B. Zaman and R. Poolla, *Opt. Mater.*, 2020, **104**, 109853.

28 D. Samanta, P. Basnet, T. I. Chanu and S. Chatterjee, *J. Alloys Compd.*, 2020, **844**, 155810.

29 N. Thomas, D. D. Dionysiou and S. C. Pillai, *J. Hazard. Mater.*, 2021, **404**, 124082.

30 P. W. Koh, L. Yuliati and S. L. Lee, *Iran. J. Sci. Technol., Trans. A: Sci.*, 2019, **43**, 95–103.

31 M. Moztahida and D. S. Lee, *J. Hazard. Mater.*, 2020, **400**, 123314.

32 M. Danish, H. Ayub, Z. A. Sandhu, A. Shoaib, S. Akram, J. Najeeb and S. Naeem, *Appl. Nanosci.*, 2021, **11**, 2503–2515.

33 L. G. De Oliveira, A. P. de Paiva, P. P. Balestrassi, J. R. Ferreira, S. C. da Costa and P. H. da Silva Campos, *Int. J. Adv. Des. Manuf. Technol.*, 2019, **104**, 1785–1837.

34 I. Veza, M. Spraggon, I. R. Fattah and M. Idris, *Results Eng.*, 2023, 101213.

35 W.-K. Chong, B.-J. Ng, L.-L. Tan and S.-P. Chai, *Energy Fuels*, 2022, **36**, 4250–4267.

36 J. Low, C. Zhang, F. Karadas and Y. Xiong, *Chin. J. Catal.*, 2023, **50**, 1–5.

37 T. Takayama, I. Tsuji, N. Aono, M. Harada, T. Okuda, A. Iwase, H. Kato and A. Kudo, *Chem. Lett.*, 2017, **46**, 616–619.

38 Y. Ren, D. Zeng and W.-J. Ong, *Chin. J. Catal.*, 2019, **40**, 289–319.

39 P. Guo, D. Zhang, X. Liu, W. Liu, R. Wang, Z. Zhang and S. Qiu, *J. Alloys Compd.*, 2022, **921**, 166066.

40 Z. Wu, Z. Xiong and B. Lai, *Environ. Funct. Mater.*, 2022, **1**(3), 298–315.

41 B. Li, F. Wang, K. Wang, J. Qiao, D. Xu, Y. Yang, X. Zhang, L. Lyu, W. Liu and J. Liu, *J. Mater. Sci. Technol.*, 2022, **104**, 244–268.

42 T. Eisa, M. A. Abdelkareem, D. A. Jadhav, H. O. Mohamed, E. T. Sayed, A. G. Olabi, P. Castaño and K.-J. Chae, *Prog. Energy Combust. Sci.*, 2023, **94**, 101044.

43 X.-X. Ji, L. Yang, Y.-L. Liu, Y. Fu and F. Ye, *Inorg. Chim. Acta*, 2023, **545**, 121244.

44 K. Ao, Q. Wei and W. A. Daoud, *ACS Appl. Mater. Interfaces*, 2020, **12**, 33595–33602.

45 G. de Souza Dias, J. M. Costa and A. F. de Almeida Neto, *Adv. Colloid Interface Sci.*, 2023, 102891.

46 S. Wang, X. He, S. Wang, X. Huang, M. Wu and D. Xiang, *Electrochim. Acta*, 2023, **441**, 141790.

47 G. Murugadoss, S. Salla, M. R. Kumar, N. Kandhasamy, H. Al Garalleh, M. Garaleh, K. Brindhadevi and A. Pugazhendhi, *Environ. Res.*, 2023, 115171.

48 N. Abid, A. M. Khan, S. Shujait, K. Chaudhary, M. Ikram, M. Imran, J. Haider, M. Khan, Q. Khan and M. Maqbool, *Adv. Colloid Interface Sci.*, 2022, **300**, 102597.

49 L. Krishnia, P. Thakur and A. Thakur, *Synthesis and Applications of Nanoparticles*, Springer, 2022, pp. 45–59.

50 P. F. de Oliveira, R. M. Torresi, F. Emmerling and P. H. Camargo, *J. Mater. Chem. A*, 2020, **8**, 16114–16141.

51 A. M. El-Khawaga, A. Zidan and A. I. Abd El-Mageed, *J. Mol. Struct.*, 2023, 135148.

52 M. Aydin, A. S. Ahsen and R. Demir-Cakan, *J. Solid State Electrochem.*, 2023, 1–10.

53 W. Zhong, J. Hong, C. Wang, Z. Li, J. Chen and S. Dmytro, *Ionics*, 2023, **29**, 917–930.

54 P. R. Nair, C. R. S. Ramirez, M. A. G. Pinilla, B. Krishnan, D. A. Avellaneda, R. F. C. Pelaes and S. Shaji, *Appl. Surf. Sci.*, 2023, 157096.

55 A. Nyabadza, M. Vazquez and D. Brabazon, *Crystals*, 2023, **13**, 253.

56 P. G. Jamkhande, N. W. Ghule, A. H. Bamer and M. G. Kalaskar, *J. Drug Delivery Sci. Technol.*, 2019, **53**, 101174.

57 B. Kanrar, K. Sanyal and R. V. Pai, *J. Anal. At. Spectrom.*, 2022, **37**, 741–749.

58 L. O. Amaral and A. L. Daniel-da-Silva, *Molecules*, 2022, **27**, 6782.

59 S. Wang, T. Wang, X. Kong, X. Zhao, H. Gan, X. Wang, Q. Meng, F. He, P. Yang and Z. Liu, *J. Colloid Interface Sci.*, 2023, **630**, 204–211.

60 S. S. Hossain, A. F. A. Rahman, A. Arsad, A. Basu, A. L. Pang, Z. Harun, M. M. A. Alwi and S. S. Ali, *Polymers*, 2023, **15**, 1528.

61 V. Ganesh, T. AlAbdulaal and I. Yahia, *Phys. Scr.*, 2023, **98**, 045908.

62 I. Ijaz, E. Gilani, A. Nazir and A. Bukhari, *Green Chem. Lett. Rev.*, 2020, **13**, 223–245.

63 A. Fathy, A. Wagih and A. Abu-Oqail, *Ceram. Int.*, 2019, **45**, 2319–2329.

64 A. Meng, W. Tian, H. Yang, X. Wang, X. Wang and Z. Li, *J. Hazard. Mater.*, 2021, **413**, 125400.

65 H. Yu, H. Huang, K. Xu, W. Hao, Y. Guo, S. Wang, X. Shen, S. Pan and Y. Zhang, *ACS Sustainable Chem. Eng.*, 2017, **5**, 10499–10508.

66 A. Hadi, J. Zahirifar, J. Karimi-Sabet and A. Dastbaz, *Ultrason. Sonochem.*, 2018, **44**, 204–214.

67 A. B. Workie, H. S. Ningsih and S.-J. Shih, *J. Anal. Appl. Pyrolysis*, 2023, 105915.

68 Y. Lee, T. Fujimoto, S. Yamanaka and Y. Kuga, *Adv. Powder Technol.*, 2021, **32**, 1619–1626.

69 G. Gahlawat and A. R. Choudhury, *RSC Adv.*, 2019, **9**, 12944–12967.

70 D. Devi, N. M. Julkapli, S. Sagadevan and M. R. Johan, *Inorg. Chem. Commun.*, 2023, 110700.

71 S. Munyai and N. Hintsho-Mbita, *Curr. Res. Green Sustainable Chem.*, 2021, **4**, 100163.

72 M. Ahmaruzzaman and V. Gadore, *J. Environ. Chem. Eng.*, 2021, **9**, 105836.

73 M. M. Gul, K. S. Ahmad, A. G. Thomas and S. M. Ibrahim, *Opt. Mater.*, 2023, **138**, 113682.

74 M. Abdullah, P. John, M. N. Ashiq, S. Manzoor, M. I. Ghori, M. U. Nisa, A. G. Abid, K. Y. Butt and S. Ahmed, *Nanotechnol. Environ. Eng.*, 2023, **8**, 63–73.

75 G. M. Neelgund, S. F. Aguilar, E. A. Jimenez and R. L. Ray, *Catalysts*, 2023, **13**, 476.

76 Z. Ali, Q. Hussain, M. A. Yawer, M. Mehmood, R. Hussain, A. Shah, H. Kanwal, A. Yawer, S. Ahmad and S. Zahid, *J. Mol. Struct.*, 2023, 134929.

77 K. H. Do, D. P. Kumar, P. Rangappa, J. Lee, S. Yun and T. K. Kim, *J. Mater. Chem. A*, 2023, **11**, 8392–8403.

78 M. Liu, A. Sheardy, G. Pathiraja, F. Tukur, A. Jayapalan and J. Wei, *Cleaner Chem. Eng.*, 2023, 100093.

79 C. Ameta, Y. Vyas and P. Chundawat, *Quantum Dots*, Elsevier, 2023, pp. 115–145.

80 M. Şaylan, B. Metin, H. Akbıyık, F. Turak, G. Çetin and S. Bakırdere, *J. Food Compos. Anal.*, 2023, **115**, 104965.

81 S. Iravani, H. Korbekandi, S. V. Mirmohammadi and B. Zolfaghari, *Res. Pharm. Sci.*, 2014, **9**, 385.

82 W. Zhu, Y. Cheng, C. Wang, N. Pinna and X. Lu, *Nanoscale*, 2021, **13**, 9112–9146.

83 C. Sambathkumar, V. Manirathinam, A. Manikandan, M. Krishna Kumar, S. Sudhahar and P. Devendran, *J. Mater. Sci.: Mater. Electron.*, 2021, **32**, 20827–20843.

84 P. Rao, S. Kumar, N. Raje, R. Tokas and N. Sahoo, *Mater. Res. Bull.*, 2016, **79**, 105–114.

85 S. Sheikhi, M. Aliannezhadi and F. S. Tehrani, *Mater. Today Commun.*, 2023, **34**, 105103.

86 P. Jeya, S. Keerthana, L. Kungumadevi, R. Yuvakkumar, G. Ravi, A. Kandasami and T. Senthil, *Environ. Res.*, 2023, **226**, 115651.

87 Z. H. Jabbar, B. H. Graimed, A. A. Okab, M. M. Alsunbuli and R. A. Al-husseiny, *J. Photochem. Photobiol., A*, 2023, 114734.

88 M. Q. He, Y. Ai, W. Hu, L. Guan, M. Ding and Q. Liang, *Adv. Mater.*, 2023, 2211915.

89 S. V. P. Vattikuti and C. Byon, *Nanoscaled Films Layers*, 2017, **239**, DOI: 10.5772/67825.

90 C. S. Torres-Castillo and J. R. Tavares, *Can. J. Chem. Eng.*, 2023, **101**, 1410–1420.

91 J. H. Chung, N. Baek, H. Lim, C. Seo, Y. K. Cho, D. Jung and D. H. Han, *Invest. Clin. Urol.*, 2023, **64**, 175–181.

92 Z. Luo, X. Lin, L. Tang, Y. Feng, Y. Gui, J. Zhu, W. Yang, D. Li, L. Zhou and L. Fu, *ACS Appl. Mater. Interfaces*, 2020, **12**, 34755–34762.

93 Y. Wu, S. Wang and K. Komvopoulos, *J. Mater. Res.*, 2020, **35**, 76–89.

94 S. Luo, C. P. Cullen, G. Guo, J. Zhong and G. S. Duesberg, *Appl. Surf. Sci.*, 2020, **508**, 145126.

95 S. S. Salem, *Arch. Microbiol.*, 2023, **205**, 128.

96 P. Narayanan, S. Divijendra Natha Reddy and P. Rao, *Modern Approaches in Waste Bioremediation: Environmental Microbiology*, Springer, 2023, pp. 251–263.

97 G. K. Sodhi and S. Saxena, *Environ. Exp. Bot.*, 2023, **209**, 105312.

98 J. Loa, I. Cruz-Rodríguez and N. Rojas-Avelizapa, *Appl. Biochem. Biotechnol.*, 2023, 1–16.

99 J. L. Lopez-Miranda, G. A. Molina, M. A. González-Reyna, B. L. España-Sánchez, R. Esparza, R. Silva and M. Estévez, *Int. J. Mol. Sci.*, 2023, **24**, 1474.

100 S. S. Salem and A. Fouda, *Biol. Trace Elem. Res.*, 2021, **199**, 344–370.

101 V. Bianchi, T. Carey, L. Viti, L. Li, E. H. Linfield, A. G. Davies, A. Tredicucci, D. Yoon, P. G. Karagiannidis and L. Lombardi, *Nat. Commun.*, 2017, **8**, 15763.

102 S. Mohammadi, J. Poostforooshan, M. F. Stodt, V. Olszok, J. Kiefer, U. Fritsching and A. P. Weber, *Appl. Energy Combust. Sci.*, 2023, 100151.

103 G. Yang and S.-J. Park, *Materials*, 2019, **12**, 1177.

104 S. Mondal, G. Hoang, P. Manivasagan, M. S. Moorthy, T. T. V. Phan, H. H. Kim, T. P. Nguyen and J. Oh, *Ceram. Int.*, 2019, **45**, 2977–2988.

105 M. d P. Yeste, C. Fernández-Ponce, E. Félix, M. Tinoco, R. Fernández-Cisnal, C. García-Villar, C. Pfaff, J. Kriwet, E. Natividad and M. Cauqui, *Ceram. Int.*, 2022, **48**, 31191–31202.

106 L. L. Félix, J. M. Porcel, F. F. H. Aragón, D. G. Pacheco-Salazar and M. H. Sousa, *SN Appl. Sci.*, 2021, **3**, 1–10.

107 M. Yaseen, M. Humayun, A. Khan, M. Usman, H. Ullah, A. A. Tahir and H. Ullah, *Energies*, 2021, **14**, 1278.

108 H. Chopra, S. Bibi, I. Singh, M. M. Hasan, M. S. Khan, Q. Yousafi, A. A. Baig, M. M. Rahman, F. Islam and T. B. Emran, *Front. Bioeng. Biotechnol.*, 2022, **10**, 548.

109 Y. Yuan, L. Wang and L. Gao, *Front. Chem.*, 2020, **8**, 818.

110 F. Qi, K.-J. Jeong, J. Gong and Z. Tang, *Acc. Chem. Res.*, 2022, **55**, 2425–2438.

111 L. Li, J. Su, J. Lu and Q. Shao, *Chem. - Asian J.*, 2023, **18**, e202201044.

112 M. A. Farhana, A. Manjceevan and J. Bandara, *J. Sci.: Adv. Mater. Devices*, 2023, 100533.

113 Y. Liu, M. Ji and P. Wang, *Mol. Pharmaceutics*, 2019, **16**, 3322–3332.

114 B. Poornaprakash, U. Chalapathi, M. Kumar, S. P. Vattikuti, B. Rajitha, P. Poojitha and S.-H. Park, *Mater. Sci. Semicond. Process.*, 2021, **121**, 105395.

115 A. Sharma, P. R. Makgwane, E. Lichtfouse, N. Kumar, A. H. Bandegharaei and M. Tahir, *Environ. Sci. Pollut. Res.*, 2023, 1–17.

116 S. Krithika and J. Balavijayalakshmi, *Inorg. Chem. Commun.*, 2022, 110324.

117 R. Zhang, F. Kiessling, T. Lammers and R. M. Pallares, *Drug Delivery Transl. Res.*, 2023, **13**, 378–385.

118 S. Ravikumar, D. Mani, E. Chicardi, R. Sepúlveda, K. Balu, V. Pandiyan and Y.-H. Ahn, *Ceram. Int.*, 2023, **49**, 9551–9559.

119 M. N. Kaka, N. Borah, A. K. Guha and C. Tamuly, *Inorg. Chem. Commun.*, 2023, 110868.

120 P. Ajibade, N. Mkhwanazi and L. Mphahlele, *Chalcogenide Lett.*, 2021, **18**, 339–349.

121 R. Afeesh, N. A. Barakat, S. S. Al-Deyab, A. Yousef and H. Y. Kim, *Colloids Surf., A*, 2012, **409**, 21–29.

122 S. Ali, F. Akbar Jan, R. Ullah and N. Ullah, *Water Sci. Technol.*, 2022, **85**, 1040–1052.

123 A. Puhan, B. Bhushan, S. Satpathy, S. Meena, A. Nayak and D. Rout, *Appl. Surf. Sci.*, 2019, **493**, 593–604.

124 P. A. Ajibade and A. E. Oluwalana, *Nanomaterials*, 2021, **11**, 2000.

125 R. Mohammed, M. E. M. Ali, E. Gomaa and M. Mohsen, *Sci. Rep.*, 2022, **12**, 18153.

126 X. Li, J. Wang, J. Zhang, C. Zhao, Y. Wu and Y. He, *J. Colloid Interface Sci.*, 2022, **607**, 412–422.

127 K. Meena and M. Shanthi, *Sustainability*, 2022, **14**, 15325.

128 N. Kandhasamy, G. Murugadoss, T. Kannappan, K. Kirubaharan and R. Kumar Manavalan, *Sustainability*, 2022, **14**, 16184.

129 T. Senasu, N. Ruengchai, S. Khamdon, N. Lorwanishpaisarn and S. Nanan, *Molecules*, 2022, **27**, 7944.

130 Z. Shalabayev, M. Baláž, N. Khan, Y. Nurlan, A. Augustyniak, N. Daneu, B. Tatykayev, E. Dutková, G. Burashev and M. Casas-Luna, *Nanomaterials*, 2022, **12**, 1250.

131 L. Isac, C. Cazan, L. Andronic and A. Enesca, *Catalysts*, 2022, **12**, 1135.

132 Y. Wang, F. Jiang, J. Chen, X. Sun, T. Xian and H. Yang, *Nanomaterials*, 2020, **10**, 178.

133 P. K. Boruah, B. Sharma, I. Karbhal, M. V. Shelke and M. R. Das, *J. Hazard. Mater.*, 2017, **325**, 90–100.

134 M. Iqbal, A. Ali, N. A. Nahyoon, A. Majeed, R. Pothu, S. Phulpoto and K. H. Thebo, *Mater. Sci. Energy Technol.*, 2019, **2**, 41–45.

135 H. Sabeeh, S. Musaddiq, M. Shahid, M. A. Khan, M. Sher and M. F. Warsi, *Mater. Res. Express*, 2018, **5**, 065062.

136 M. Rani and U. J. Shanker, *Chem. Eng. J.*, 2018, **348**, 754–764.

137 C.-Y. Zou, W.-C. Ji, S.-Q. Liu, Z. Shen, Y. Zhang and N.-S. Jiang, *Chin. J. Catal.*, 2018, **39**, 1051–1059.

138 E. E. El-Katori, M. Ahmed, A. El-Bindary and A. M. Oraby, *J. Photochem. Photobiol., A*, 2020, **392**, 112403.

139 S. Janbandhu, A. Joshi, S. Munishwar and R. Gedam, *Appl. Surf. Sci.*, 2019, **497**, 143758.

140 Y. Chen, B. Zhai, Y. Liang, Y. Li and J. Li, *J. Solid State Chem.*, 2019, **274**, 32–39.

141 T. Senasu, T. Chankhanittha, K. Hemavibool and S. Nanan, *Mater. Sci. Semicond. Process.*, 2021, **123**, 105558.

142 K. A. Adegoke, M. Iqbal, H. Louis and O. S. Bello, *Mater. Sci. Energy Technol.*, 2019, **2**, 329–336.

143 J. You, L. Wang, W. Bao, A. Yan and R. Guo, *J. Mater. Sci.*, 2021, **56**, 6732–6744.

144 M. Junaid, M. Imran, M. Ikram, M. Naz, M. Aqeel, H. Afzal, H. Majeed and S. Ali, *Appl. Nanosci.*, 2019, **9**, 1593–1602.

145 M. Zhang, H.-f Yin, J.-c Yao, M. Arif, B. Qiu, P.-f Li and X.-h Liu, *Colloids Surf., A*, 2020, **602**, 124778.

146 P. Nandi and D. Das, *J. Phys. Chem. Solids*, 2022, **160**, 110344.

147 C. Nethravathi, J. T. Rajamathi and M. Rajamathi, *ACS Omega*, 2019, **4**, 4825–4831.

148 P. Lakshmanan, S. Thirumaran and S. Ciattini, *J. Mol. Struct.*, 2020, **1220**, 128704.

149 H. Hafdi, J. Mouldar, M. Joudi, B. Hatimi, H. Nasrellah, M. A. E. Mhammedi and M. Bakasse, *Opt. Quantum Electron.*, 2021, **53**, 1–13.

150 S. Thirumaran, G. Gurumoorthy, R. Arulmozhi and S. Ciattini, *Appl. Organomet. Chem.*, 2020, **34**, e5761.

151 S. Kokilavani, A. A. Al-Kheraif, A. M. Thomas, A. Syed, A. M. Elgorban, L. L. Raju, A. Das and S. S. Khan, *Phys. E*, 2021, **133**, 114767.

152 V. Manikandan, R. Elancheran, P. Revathi, P. Suganya and K. Krishnasamy, *Bull. Mater. Sci.*, 2020, **43**, 1–10.

153 S. Muninathan and S. Arumugam, *Int. J. Hydrogen Energy*, 2021, **46**, 6532–6546.

154 N. A. Marand, S. Masoudpanah and M. S. Bafghi, *Ceram. Int.*, 2018, **44**, 17277–17282.

155 Y. Li, X. Li, X.-T. Wang, L.-J. Jian, N. I. M. Abdallah, X.-F. Dong and C.-W. Wang, *Colloids Surf., A*, 2021, **608**, 125565.

156 R. Khan, N. S. Das, B. Das, B. Das and K. K. Chattopadhyay, *J. Photochem. Photobiol., A*, 2021, **412**, 113212.

157 Y. Qi, J. Xu, M. Zhang, H. Lin and L. Wang, *Int. J. Hydrogen Energy*, 2019, **44**, 16336–16347.

158 P. Arumugam, P. Sengodan, N. Duraisamy, R. Rajendran and V. Vasudevan, *Ionics*, 2020, **26**, 4201–4212.

159 N. Ardebilchi Marand, S. Masoudpanah, M. S. Bafghi and S. Alamolhoda, *J. Electron. Mater.*, 2020, **49**, 1266–1272.

160 K. Arathi, T. Ravishankar, K. Raj and K. Nagashree, *Chem. Pap.*, 2021, **75**, 4707–4718.

161 S. Zhao, J. Xu, Z. Li, Z. Liu and Y. Li, *J. Colloid Interface Sci.*, 2019, **555**, 689–701.

162 G. Gurumoorthy, R. Hema and M. Sundararajan, *Annals of the Romanian Society for Cell Biology*, 2021, 2086–2090.

163 G. Gurumoorthy, R. Hema and M. Sundararajan, *Annals of the Romanian Society for Cell Biology*, 2021, 2096–2099.

164 I. Mukhtar, S. Ali, S. Jamil and S. R. Khan, *Chem. Phys. Lett.*, 2020, **754**, 137649.

165 S. M. Pourmortazavi, M. Rahimi-Nasrabadi, B. Larijani, M. S. Karimi and S. Mirsadeghi, *J. Mater. Sci.: Mater. Electron.*, 2018, **29**, 13833–13841.

166 M. Sohail, J. Huang, Z. Lai, Y. Cao, S. Ruan, M. N. Shah, F. U. Khan, H. I. A. Qazi and B. Ullah, *J. Inorg. Organomet. Polym. Mater.*, 2020, **30**, 5168–5179.

167 M. Danish and M. Muneer, *Ceram. Int.*, 2021, **47**, 13043–13056.

168 A. Chowdhury, S. Kumari, A. A. Khan and S. Hussain, *J. Hazard. Mater.*, 2020, **385**, 121602.

169 M. A. Khan, W. Hussain, K. Tufail, M. Sulaman, A. R. Ayub, W. A. Khan and H. Li, *Energy Rep.*, 2021, **7**, 7615–7627.

170 M. I. Din, R. Khalid, J. Najeeb and Z. Hussain, *J. Cleaner Prod.*, 2021, **298**, 126567.

171 M. Hosseini, N. Fazelian, A. Fakhri, H. Kamyab, K. K. Yadav and S. Chelliapan, *J. Photochem. Photobiol., B*, 2019, **194**, 128–134.

172 D. Ayodhya and G. Veerabhadram, *Mater. Today Energy*, 2018, **9**, 83–113.

173 X. Zheng, Y. Dong and T. Liu, *Colloids Surf., A*, 2020, **598**, 124854.

174 R. Chaudhary, S. C. Ameta and R. Ameta, *Maced. J. Chem. Chem. Eng.*, 2019, **38**, 107–114.

175 A. Chowdhury, A. A. Khan, S. Kumari and S. Hussain, *ACS Sustainable Chem. Eng.*, 2019, **7**, 4165–4176.

176 S. Kokilavani, A. Syed, H. A. AL-Shwaiman, M. M. Alkhulaifi, F. N. Almajdhi, A. M. Elgorban and S. S. Khan, *Colloid Interface Sci. Commun.*, 2021, **42**, 100415.

177 M. A. Abid, D. A. Abid, W. J. Aziz and T. M. Rashid, *Phys. B*, 2021, **622**, 413277.

178 J. Li and W. B. Ko, *Elastomers Compos.*, 2018, **53**, 75–79.

179 S. B. Atla, W.-R. Lin, T.-C. Chien, M.-J. Tseng, J.-C. Shu, C.-C. Chen and C.-Y. Chen, *Mater. Chem. Phys.*, 2018, **216**, 380–386.

180 S. Baek, Y. Ghaffari and J. Bae, *Catalysts*, 2022, **12**, 1045.

181 P. K. Boruah, B. Sharma, I. Karbhal, M. V. Shelke and M. R. Das, *J. Hazard. Mater.*, 2017, **325**, 90–100.

182 S. Das, A. Samanta and S. Jana, *ACS Sustainable Chem. Eng.*, 2017, **5**, 9086–9094.

183 F. Davar, A. Majedi and A. Abbasi, *J. Mater. Sci.: Mater. Electron.*, 2017, **28**, 4871–4878.

184 O. Długosz, K. Szostak, M. Krupiński and M. Banach, *Int. J. Environ. Sci. Technol.*, 2021, **18**, 561–574.

185 S. Douafer, H. Lahmar, M. Benamira, G. Rekhila and M. Trari, *J. Phys. Chem. Solids*, 2018, **118**, 62–67.

186 M. Dubey, N. V. Challagulla, S. Wadhwa and R. Kumar, *Colloids Surf., A*, 2021, **609**, 125720.

187 D. P. Dutta, M. Ramakrishnan, M. Roy and A. Kumar, *J. Photochem. Photobiol., A*, 2017, **335**, 102–111.

188 Z.-T. Hu, J. Liu, X. Yan, W.-D. Oh and T.-T. Lim, *Chem. Eng. J.*, 2015, **262**, 1022–1032.

189 F. Iazdani and A. Nezamzadeh-Ejhieh, *Chem. Phys.*, 2021, **550**, 111305.

190 K. Kirchberg, A. Becker, A. Bloesser, T. Weller, J. Timm, C. Suchomski and R. Marschall, *J. Phys. Chem. C*, 2017, **121**, 27126–27138.

191 M. A. J. Kouhbanani, N. Beheshtkhoo, A. M. Amani, S. Taghizadeh, V. Beigi, A. Z. Bazmandeh and N. Khalaf, *Mater. Res. Express*, 2018, **5**, 115013.

192 Y. Li, X.-T. Wang, X.-Q. Zhang, X. Li, J. Wang and C.-W. Wang, *Phys. E*, 2020, **118**, 113865.

193 Y. Liu, L. Zong, C. Zhang, W. Liu, A. Fakhri and V. K. Gupta, *Surf. Interfaces*, 2021, **26**, 101292.

194 S. Lohrasbi, M. A. J. Kouhbanani, N. Beheshtkhoo, Y. Ghasemi, A. M. Amani and S. Taghizadeh, *Bionanoscience*, 2019, **9**, 317–322.

195 N. Madubuonu, S. O. Aisida, A. Ali, I. Ahmad, T.-K. Zhao, S. Botha, M. Maaza and F. I. Ezema, *J. Photochem. Photobiol., B*, 2019, **199**, 111601.

196 S. Mortazavi-Derazkola, M. Salavati-Niasari, O. Amiri and A. Abbasi, *J. Energy Chem.*, 2017, **26**, 17–23.

197 H. Muthukumar and M. Matheswaran, *ACS Sustainable Chem. Eng.*, 2015, **3**, 3149–3156.

198 A. C. Pradhan, B. Nanda, K. Parida and G. R. Rao, *J. Phys. Chem. C*, 2015, **119**, 14145–14159.

199 S. Qasim, A. Zafar, M. S. Saif, Z. Ali, M. Nazar, M. Waqas, A. U. Haq, T. Tariq, S. G. Hassan and F. Iqbal, *J. Photochem. Photobiol., B*, 2020, **204**, 111784.

200 M. Rani and U. Shanker, *Chem. Eng. J.*, 2018, **348**, 754–764.

201 H. Sabeeh, S. Musaddiq, M. Shahid, M. A. Khan, M. Sher and M. F. Warsi, *Mater. Res. Exp.*, 2018, **5**, 065062.

202 N. Shaheen, M. A. Yousuf, I. Shakir, S. Zulfiqar, P. O. Agboola and M. F. Warsi, *Phys. B*, 2020, **580**, 411820.

203 S. Vignesh, M. Sivakami, P. Muniyappan and J. K. Sundar, *Int. Res. J. Eng. Technol.*, 2017, **4**, 70.

204 G. Zhao, Z. Mo, P. Zhang, B. Wang, X. Zhu and R. Guo, *J. Porous Mater.*, 2015, **22**, 1245–1253.

205 C.-Y. Zou, W.-C. Ji, S.-Q. Liu, Z. Shen, Y. Zhang and N.-S. Jiang, *Chin. J. Catal.*, 2018, **39**, 1051–1059.

206 C. Behera, S. P. Ghosh, J. P. Kar and S. L. Samal, *New J. Chem.*, 2020, **44**, 11684–11693.

207 N. Tahir, M. Zahid, A. Jillani, M. Yaseen and Q. Abbas, *J. Photochem. Photobiol., A*, 2023, **436**, 114376.

208 G. Luna-López, M. Del Barrio, J. Fize, V. Artero, A. M. Coito, I. A. Pereira, J. C. Conesa, A. Iglesias-Juez, A. L. De Lacey and M. Pita, *Bioelectrochemistry*, 2023, **150**, 108361.

209 M. A. Al-Nuaim, A. A. Alwasiti and Z. Y. Shnain, *Chem. Pap.*, 2023, **77**, 677–701.

210 W. Fu, J. Fan and Q. Xiang, *Chin. J. Struct. Chem.*, 2022, **41**, 2206039–2206047.

211 S. Han, B. Li, L. Huang, H. Xi, Z. Ding and J. Long, *Chin. J. Struct. Chem.*, 2022, **41**, 2201007–2201013.

212 H. Leelavathi, R. Muralidharan, N. Abirami, S. Tamizharasan, S. Sankeetha, A. Kumarasamy and R. Arulmozhi, *Colloids Surf., A*, 2023, **656**, 130449.

213 L.-H. Kao, K.-S. Chuang, H. N. Catherine, J.-H. Huang, H.-J. Hsu, Y.-C. Shen and C. Hu, *J. Taiwan Inst. Chem. Eng.*, 2023, **142**, 104638.
214 M. Lyulyukin, N. Kovalevskiy, A. Bukhtiyarov, D. Kozlov and D. Selishchev, *Int. J. Mol. Sci.*, 2023, **24**, 5693.
215 R. Sinha and P. S. Ghosal, *J. Environ. Manage.*, 2023, **328**, 117011.
216 C. Yuan, H. Lv, Y. Zhang, Q. Fei, D. Xiao, H. Yin, Z. Lu and Y. Zhang, *Carbon*, 2023, **206**, 237–245.
217 W. Jin, L. Jing, X. Wu, R. Ying-Yi and W. Feng, *Acta Phys.-Chim. Sin.*, 2021, **37**, DOI: 10.3866/PKU.WHXB202008043.
218 Q. Husain, *Crit. Rev. Biotechnol.*, 2006, **26**, 201–221.
219 E. Forgacs, T. Cserháti and G. Oros, *Environ. Int.*, 2004, **30**, 953–971.
220 N. Patel Jay, K. Vaishnav Darshit, R. Joshi Pavan and R. Tipre Devayani, *Res. J. Chem. Environ.*, 2023, **27**, 4.
221 M. Sukumar, J. R. Rajabathar, H. Al-Lohedan, S. Suresh, C. S. Dash, M. Sundararajan, P. S. Subudhi, S. Arokiyaraj, E. Yanmaz and S. Yuvaraj, *J. Alloys Compd.*, 2023, 169902.
222 E. Turcu, C. G. Coromelci, V. Harabagiu and M. Ignat, *Catalysts*, 2023, **13**, 345.
223 T. Islam, M. R. Repon, T. Islam, Z. Sarwar and M. M. Rahman, *Environ. Sci. Pollut. Res.*, 2023, **30**, 9207–9242.
224 D. Sannino, N. Morante, O. Sacco, A. Mancuso, L. De Guglielmo, G. Di Capua, N. Femia and V. Vaiano, *Photochem. Photobiol. Sci.*, 2023, **22**, 185–193.
225 Z. Ma, Y. Han, F. Xu and X. Wang, *Int. J. Biol. Macromol.*, 2023, 124265.
226 T. Amber, S. Nosheen, R. Kamran, S. Kiran, M. I. Yousaf, N. Sharifi and S. Riazi, *Pak. J. Sci. Ind. Res., Ser. A*, 2023, **66**, 16–22.
227 C. Han, C. Cheng, F. Liu, X. Li, G. Wang and J. Li, *Nanotechnol. Rev.*, 2023, **12**, 20220503.
228 A. Qayoom, I. Ashraf, A. Rashid, M. Ayoub and D. Kumar, 2022.
229 R. Mugumoa, E. O. Ichipi, S. M. Tichapondwa and E. MN, 2023.
230 V. Dileepkumar, P. Surya, C. Pratapkumar, R. Viswanatha, C. Ravikumar, M. A. Kumar, H. Muralidhara, I. M. Al-Akraa, A. M. Mohammad and Z. Chen, *J. Environ. Chem. Eng.*, 2020, **8**, 104005.
231 T. T. Xuan, L. N. Long and T. Van Khai, *Vietnam J. Chem.*, 2020, **58**, 92–100.
232 S. Munyai, Z. Tetana, M. Mathipa, B. Ntsendwana and N. Hintsho-Mbita, *Optik*, 2021, **247**, 167851.
233 M. Mahanthappa, N. Kottam and S. Yellappa, *Appl. Surf. Sci.*, 2019, **475**, 828–838.
234 B. Ren, W. Shen, L. Li, S. Wu and W. Wang, *Appl. Surf. Sci.*, 2018, **447**, 711–723.
235 F. Soltani-Nezhad, A. Saljooqi, A. Mostafavi and T. Shamspur, *Ecotoxicol. Environ. Saf.*, 2020, **189**, 109886.
236 F. Karimi, H. R. Rajabi and L. Kavoshi, *Ultrason. Sonochem.*, 2019, **57**, 139–146.
237 A. Alharbi, R. K. Shah, A. Sayqal, A. Subaihi, A. A. Alluhaybi, F. K. Algethami, A. M. Naglah, A. A. Almehizia, H. A. Katouah and H. M. Youssef, *Alexandria Eng. J.*, 2021, **60**, 2167–2178.
238 A. M. Palve and D. N. Kokil, *Mater. Res. Express*, 2019, **6**, 105536.
239 J. Varghese, *J. Phys. Chem. Solids*, 2021, **156**, 109911.
240 N. Tavker and M. Sharma, *J. Environ. Manage.*, 2020, **255**, 109906.
241 E. B. Yazdani and A. Mehrizad, *J. Mol. Liq.*, 2018, **255**, 102–112.
242 Z. Ahmadi, H. Ramezani, S. N. Azizi and M. J. Chaichi, *Environ. Sci. Pollut. Res.*, 2020, **27**, 9707–9717.
243 A. G. Raju, B. D. Rao, G. Himabindu and S. M. Botsa, *J. Mater. Res. Technol.*, 2022, **17**, 2648–2656.
244 H. D. Shelke, A. R. Machale, A. A. Surwase, S. F. Shaikh, A. U. H. S. Rana and H. M. Pathan, *Coatings*, 2023, **13**, 522.
245 O. F. Er, A. Caglar, B. Ulas, H. Kivrak and A. Kivrak, *Mater. Chem. Phys.*, 2020, **241**, 122422.
246 P. O. Agboola and I. Shakir, *J. Mater. Res. Technol.*, 2022, **18**, 4303–4313.
247 H. Shen, Z. Shao, Q. Zhao, M. Jin, C. Shen, M. Deng, G. Zhong, F. Huang, H. Zhu and F. Chen, *J. Colloid Interface Sci.*, 2020, **573**, 115–122.
248 Q. Lei, S. Yang, D. Ding, J. Tan, J. Liu and R. Chen, *J. Mater. Chem. A*, 2021, **9**, 2491–2525.
249 X. Zhang, W. Huang, L. Yu, M. García-Melchor, D. Wang, L. Zhi and H. Zhang, *Carbon Energy*, 2022, e362.
250 Y. Zhang, Y. Shen, J. Liu, L. Lv, M. Zhou, X. Yang, X. Meng and Z. Zhou, *Appl. Phys. Lett.*, 2023, **122**, DOI: 10.1063/5.0127150.
251 C. Hu, S. Tu, N. Tian, T. Ma, Y. Zhang and H. Huang, *Angew. Chem., Int. Ed.*, 2021, **60**, 16309–16328.
252 Y. Su, L. Zhang, W. Wang and D. Shao, *ACS Sustainable Chem. Eng.*, 2018, **6**, 8704–8710.
253 T.-Y. Chen, Y. W. Hsiao, M. Baker-Fales, F. Cameli, P. Dimitrakellis and D. G. Vlachos, *Chem. Sci.*, 2022, **13**, 10644–10685.
254 R. Wang, J. Shen, W. Zhang, Q. Liu, M. Zhang and H. Tang, *Ceram. Int.*, 2020, **46**, 23–30.
255 G. Zhang, L. Li, Z.-J. Zhao, T. Wang and J. Gong, *Acc.Mater. Res.*, 2022, **4**, 212–222.
256 X. Tu, H. Xu, C. Li, X. Liu, G. Fan and W. Sun, *Comput. Theor. Chem.*, 2021, **1203**, 113360.
257 J. Su, D. Luise, I. Ciofini and F. Labat, *J. Phys. Chem. C*, 2023, **127**, 5968–5981.
258 J. Tang, B. Gao, J. Pan, L. Chen, Z. Zhao, S. Shen, J.-K. Guo, C.-T. Au and S.-F. Yin, *Appl. Catal., A*, 2019, **588**, 117281.
259 P. Lakshmanan, R. Arulmozhi, S. Thirumaran and S. Ciattini, *Polyhedron*, 2022, **218**, 115766.
260 S. Abdpour, E. Kowsari, B. Bazri, M. R. A. Moghaddam, S. S. Tafreshi, N. H. de Leeuw, I. Simon, L. Schmolke, D. Dietrich and S. Ramakrishna, *J. Mol. Liq.*, 2020, **319**, 114341.
261 P. Lakshmanan, E. Gayathri, S. Thirumaran and S. Ciattini, *J. Mol. Struct.*, 2023, **1273**, 134306.
262 H. Wang, J. Xu, Q. Zhang, S. Hu, W. Zhou, H. Liu and X. Wang, *Adv. Funct. Mater.*, 2022, **32**, 2112362.

263 S. Awais, H. Munir, J. Najeeb, F. Anjum, K. Naseem, N. Kausar, M. Shahid, M. Irfan and N. Najeeb, *J. Cleaner Prod.*, 2023, 136916.

264 N. Tiwari, S. Chakrabortty, K. Samal, S. Moulick, B. G. Mohapatra, S. Samanta, P. Mohapatra, K. Sanjay, J. Nayak and S. Banerjee, *J. Taiwan Inst. Chem. Eng.*, 2023, 104800.

265 P. Kowsalya, S. Uma Bharathi, S. Sivasankar and M. Chamundeeswari, *J. Iran. Chem. Soc.*, 2023, 1–13.

266 S. Rastgar, H. Rezaei, H. Younesi, H. Abyar and A. Kordrostami, *Biomass Convers. Biorefin.*, 2023, 1–12.

267 R. Shakunthala and M. Matheswaran, *Opt. Mater.*, 2023, **138**, 113719.

268 A. Ebrahimi, K. Ebrahim, A. Abdolahnejad, N. Jafari, M. Karimi, A. Mohammadi and A. Nikoonahad, *Int. J. Environ. Anal. Chem.*, 2022, **102**, 7015–7032.

269 S. Mosleh, M. Rahimi, M. Ghaedi, K. Dashtian and S. Hajati, *RSC Adv.*, 2016, **6**, 63667–63680.

270 V. Mahmoodi and J. Sargolzaei, *Desalin. Water Treat.*, 2014, **52**, 6664–6672.

271 M. Lal, P. Sharma, L. Singh and C. Ram, *Results Eng.*, 2023, 100890.

272 F. Elfghi, *Chem. Eng. Res. Des.*, 2016, **113**, 264–272.

273 P. Pakravan, A. Akhbari, H. Moradi, A. H. Azandaryani, A. M. Mansouri and M. Safari, *Appl. Petrochem. Res.*, 2015, **5**, 47–59.

274 S. J. M. Breig and K. J. K. Luti, *Mater. Today: Proc.*, 2021, **42**, 2277–2284.

275 S. Karimifard and M. R. A. Moghaddam, *Sci. Total Environ*, 2018, **640**, 772–797.

276 K. Kighuta, A.-I. Gopalan, D.-E. Lee, G. Saianand, Y.-L. Hou, S.-S. Park, K.-P. Lee, J.-C. Lee and W.-J. Kim, *J. Environ. Chem. Eng.*, 2021, **9**, 106417.

277 H. Chaker, A. E. Attar, M. Djennas and S. Fourmentin, *Chem. Eng. Res. Des.*, 2021, **171**, 198–212.

278 M. H. Mahmoudian, A. Mesdaghinia, A. H. Mahvi, S. Nasseri, R. Nabizadeh and M. H. Dehghani, *J. Environ. Health Sci. Eng.*, 2022, 1–12.

279 K. Rasouli, A. Alamdari and S. Sabbaghi, *Sep. Purif. Technol.*, 2023, **307**, 122799.

280 H. Chaker, N. Ameur, K. Saidi-Bendahou, M. Djennas and S. Fourmentin, *J. Environ. Chem. Eng.*, 2021, **9**, 104584.

281 N. Mohammed, P. Palaniandy, F. Shaik, H. Mewada and D. Balakrishnan, *Chemosphere*, 2023, **314**, 137665.

282 H. Ali, M. Yasir, F. A. Ngwabebhoh, T. Sopik, O. Zandraa, J. Sevcik, M. Masar, M. Machovsky and I. Kuritka, *J. Photochem. Photobiol., A*, 2023, 114733.

283 R. Tabaraki and O. Abdi, *J. Iran. Chem. Soc.*, 2020, **17**, 839–846.

284 M. Berkani, M. K. Bouchareb, M. Bouhelassa and Y. Kadmi, *Top. Catal.*, 2020, **63**, 964–975.

285 N. Mohammed, P. Palaniandy, F. Shaik, B. Deepanraj and H. Mewada, *Environ. Res.*, 2023, 115696.

286 S. K. Kassahun, Z. Kiflie, H. Kim and A. F. Baye, *Environ. Technol. Innovation*, 2021, **23**, 101761.

287 M. Rostami, H. Mazaheri, A. Hassani Joshaghani and A. Shokri, *Int. J. Eng.*, 2019, **32**, 1074–1081.

288 B. Lee, M. Mahtab, T. Neo, I. Farooqi and A. Khursheed, *J. Water Process Eng.*, 2022, **47**, 102673.

289 A. Oulebsir, T. Chaabane, S. Zaidi, K. Omine, V. Alonzo, A. Darchen, T. Msagati and V. Sivasankar, *Arabian J. Chem.*, 2020, **13**, 271–289.

290 M. S. A. Wahab, S. Abd Rahman and R. A. Samah, *Heliyon*, 2020, **6**, e05610.

291 M. T. Luiz, J. S. R. Viegas, J. P. Abriata, F. Viegas, F. T. M. de Carvalho Vicentini, M. V. L. B. Bentley, M. Chorilli, J. M. Marchetti and D. R. Tapia-Blacido, *Eur. J. Pharm. Biopharm.*, 2021, **165**, 127–148.

292 M. Eftekhari, M. Akrami, M. Gheibi, H. Azizi-Toupkanloo, A. M. Fathollahi-Fard and G. Tian, *Environ. Sci. Pollut. Res.*, 2020, **27**, 43999–44021.

293 A. Raychaudhuri and M. Behera, *J. Hazard., Toxic Radioact. Waste*, 2020, **24**, 04020013.

294 N. Parmar and J. K. Srivastava, *J. Indian Chem. Soc.*, 2022, **99**, 100584.

295 R. Tangsiri and A. Nezamzadeh-Ejhieh, *Chem. Phys. Lett.*, 2020, **758**, 137919.

296 A. Asfaram, M. Ghaedi, F. Yousefi and M. Dastkhoon, *Ultrason. Sonochem.*, 2016, **33**, 77–89.

297 A. E. Attar, H. Chaker, M. Djennas and S. Fourmentin, *Inorg. Chem. Commun.*, 2022, 110210.

298 L. A. Meira and F. de Souza Dias, *Microchem. J.*, 2017, **130**, 56–63.

299 T. Sudha, G. Divya, J. Sujaritha and P. Duraimurugan, *J. Pharm. Res.*, 2017, **7**(8), 550–565.

300 A. Khataee, M. Kasiri and L. Alidokht, *Environ. Technol.*, 2011, **32**, 1669–1684.

301 C. Song, X. Li, L. Wang and W. Shi, *Sci. Rep.*, 2016, **6**, 1–12.

302 S. Sohrabi and F. Akhlaghian, *Process Saf. Environ. Prot.*, 2016, **99**, 120–128.

303 E. Nascimben Santos, Z. László, C. Hodúr, G. Arthanareeswaran and G. Veréb, *Asia-Pac. J. Chem. Eng.*, 2020, **15**, e2533.

304 M. Fathinia, A. Khataee, M. Zarei and S. Aber, *J. Mol. Catal. A: Chem.*, 2010, **333**, 73–84.

305 C. Sahoo and A. Gupta, *J. Hazard. Mater.*, 2012, **215**, 302–310.

306 R. Hasanzadeh, P. Mojaver, T. Azdast, S. Khalilarya and A. Chitsaz, *Int. J. Hydrogen Energy*, 2023, **48**, 5873–5886.

307 V. Shrivastava, I. Ali, M. M. Marjub, E. R. Rene and A. M. F. Soto, *Chemosphere*, 2022, **293**, 133553.

308 J. Xi, H. Sun, D. Wang, Z. Zhang, X. Duan, J. Xiao, F. Xiao, L. Liu and S. Wang, *Appl. Catal., B*, 2018, **225**, 291–297.

309 S. Chu, Y. Pan, Y. Wang, H. Zhang, R. Xiao and Z. Zou, *J. Mater. Chem. A*, 2020, **8**, 14441–14462.

310 X. Zhao, J. Feng, J. Liu, J. Lu, W. Shi, G. Yang, G. Wang, P. Feng and P. Cheng, *Adv. Sci.*, 2018, **5**, 1700590.

311 H. Zhou, X. Sheng, J. Xiao, Z. Ding, D. Wang, X. Zhang, J. Liu, R. Wu, X. Feng and L. Jiang, *J. Am. Chem. Soc.*, 2020, **142**, 2738–2743.

312 J. Wang and Z. Liu, *TrAC, Trends Anal. Chem.*, 2020, **133**, 116089.

313 Z. Qin, Y. Li and N. Gu, *Adv. Healthcare Mater.*, 2018, **7**, 1800347.

314 A. A. Barzinjy, S. M. Hamad, S. Aydın, M. H. Ahmed and F. H. Hussain, *J. Mater. Sci.: Mater. Electron.*, 2020, **31**, 11303–11316.

315 Y. Zou, B. Huang, L. Cao, Y. Deng and J. Su, *Adv. Mater.*, 2021, **33**, 2005215.

316 J. M. Aguirre-Cortés, A. I. Moral-Rodríguez, E. Bailón-García, A. Davó-Quiñonero, A. F. Pérez-Cadenas and F. Carrasco-Marín, *Appl. Mater. Today*, 2023, **32**, 101831.

317 F. Lamberti, C. Mazzariol, F. Spolaore, R. Ceccato, L. Salmaso and S. Gross, *Sustainable Chem.*, 2022, **3**, 114–130.

318 D. Tetzlaff, S. K. Carey, J. P. McNamara, H. Laudon and C. Soulsby, *Water Resour. Res.*, 2017, **53**, 2598–2604.

319 F.-Y. Chen, Z.-Y. Wu, Z. Adler and H. Wang, *Joule*, 2021, **5**, 1704–1731.

320 J. Annamalai, S. B. Ummalyma, A. Pandey and T. Bhaskar, *Environ. Sci. Pollut. Res.*, 2021, **28**, 49362–49382.

321 I. M. Fukuda, C. F. F. Pinto, C. D. S. Moreira, A. M. Saviano and F. R. Lourenço, *Braz. J. Pharm. Sci.*, 2018, **54**, DOI: 10.1590/s2175-97902018000001006.